

UNSTABLE NONRADIAL OSCILLATIONS ON HELIUM BURNING NEUTRON STARS

ANTHONY L. PIRO

Department of Physics, Broida Hall, University of California
Santa Barbara, CA 93106; piro@physics.ucsb.edu

AND

LARS BILDSTEN

Kavli Institute for Theoretical Physics and Department of Physics, Kohn Hall, University of California
Santa Barbara, CA 93106; bildsten@kitp.ucsb.edu

Draft version July 16, 2018

ABSTRACT

Material accreted onto a neutron star can stably burn in steady state only when the accretion rate is high (typically super-Eddington) or if a large flux from the neutron star crust permeates the outer atmosphere. For such situations we have analyzed the stability of nonradial oscillations, finding one unstable mode for pure helium accretion. This is a shallow surface wave which resides in the helium atmosphere above the heavier ashes of the ocean. It is excited by the increase in the nuclear reaction rate during the oscillations, and it grows on the timescale of a second. For a slowly rotating star, this mode has a frequency $\omega/(2\pi) \approx (20-30 \text{ Hz})(l(l+1)/2)^{1/2}$, and we calculate the full spectrum that a rapidly rotating ($\gg 30 \text{ Hz}$) neutron star would support. The short period X-ray binary 4U 1820–30 is accreting helium rich material and is the system most likely to show this unstable mode, especially when it is not exhibiting X-ray bursts. Our discovery of an unstable mode in a thermally stable atmosphere shows that nonradial perturbations have a different stability criterion than the spherically symmetric thermal perturbations that generate type I X-ray bursts.

Subject headings: accretion, accretion disks — stars: individual (4U 1820–30) — stars: neutron — stars: oscillations — X-rays: stars

1. INTRODUCTION

Type I X-ray bursts are caused by unstable nuclear burning on accreting neutron stars (NSs) (see recent reviews by Bildsten 1998; Strohmayer & Bildsten 2003) in low mass X-ray binaries (LMXBs). They have rise times of seconds with decay times ranging from tens to hundreds of seconds depending on the thickness and composition of the accumulated material. These bursts repeat every few hours – the timescale to accumulate an unstable amount of fuel on a NS. Evidence that nuclear burning powers the bursts is the observed ratio of the time averaged accretion luminosity to the time averaged burst luminosity (≈ 40 for hydrogen rich accretion and ≈ 125 for pure helium accretion). The thermonuclear instability which triggers these bursts is usually due to the extreme temperature sensitivity of triple- α reactions (Hansen & Van Horn 1975; Woosley & Taam 1976; Maraschi & Cavaliere 1977; Joss 1977; Lamb & Lamb 1978).

Ever since the original work of Hansen & Van Horn (1975), the approach to assessing the stability of burning on a NS has been to apply a spherically symmetric thermal perturbation to a spherical model (Schwarzschild & Härm 1965). This is either done numerically through a time-dependent code (e.g. Woosley et al. 2003), analytically with a one-zone model (e.g. Fujimoto, Hanawa & Miyaji 1981), or using an eigenvalue approach (e.g. Narayan & Heyl 2003). These results roughly agree and find a thermal runaway once a critical amount of fuel has accumulated. These calculations also find the accretion rate above which burning is stable.

We are now taking an alternative approach to this problem. Using a NS envelope that is stable to spherically symmetric thermal perturbations (i.e. not bursting), we ask whether the envelope is unstable to a non-axisymmetric perturbation. Since the immediate response to such a perturbation is a wave, the

proper way to proceed is through a study of the nonradial oscillation modes. The criterion for thermal versus mode stability is mathematically different (as we will explain in §2.2 and §3.3), but it is not yet clear how this contrast will manifest itself observationally. Nonradial oscillations in burning NS envelopes have been studied before (for example McDermott & Taam 1987; Strohmayer & Lee 1996), but these are for atmospheres that are thermally unstable, leaving our question unanswered.

To simplify this initial work, we assume that the NS is accreting pure helium and burning this fuel at the same rate it accretes. This steady state burning proceeds if the NS envelope is thermally stable (and no type I X-ray bursts are occurring). It is stable when either the temperature sensitivity of triple- α reactions has weakened due to a high envelope temperature ($\gtrsim 5 \times 10^8 \text{ K}$), or the thermal balance of the burning layer is fixed by a high flux from deeper parts of the NS (Paczynski 1983a). We then find the eigenfrequencies and test the stability of g-modes in such an envelope. The one unstable mode we find is a shallow surface wave in the helium layer that is supported by the buoyancy of the helium/carbon interface. It has a non-rotating frequency of $\omega/(2\pi) \approx (20-30 \text{ Hz})(l(l+1)/2)^{1/2}$, depending on the accretion rate. This mode is driven unstable by the ϵ -mechanism (i.e. pumped by the perturbation in nuclear burning) and grows in amplitude on the timescale of a second. This is very different from other observed stellar pulsations, such as Cepheid variables, which are driven by the κ -mechanism (pumped by changes in opacity). Unlike the damped higher radial order g-modes, the unstable mode suffers little radiative damping in the outer atmosphere. Rapid rotation like that seen from many accreting NSs (200-700 Hz) will yield multiple oscillation frequencies with a well defined pattern. If such a frequency pattern were seen from a NS it would give strong evidence that a mode has been excited.

In §2 we describe the physics of a NS star envelope accreting and burning helium in steady state. The conditions required for steady state accretion are reviewed. Nonradial adiabatic oscillations in a plane-parallel envelope are discussed in §3, and though much of this has been described in previous papers, we include additional details and strategies that are relevant for NSs. The oscillatory equations are derived in §3.1, and in §3.2 we calculate the radial eigenfunctions and find the g-mode frequencies for a non-rotating NS. The stability of these modes is investigated in §3.3, including a look at excitation and damping times. In §3.4 we find the unstable mode’s frequency on a rapidly rotating neutron star. The LMXB 4U 1820–30 is discussed in §4 along with other candidates that might show the excited mode we have found. We conclude in §5 by summarizing our findings and discussing future directions for this work.

2. STEADY STATE HELIUM ACCRETION

In solving for a NS envelope we closely follow the model described by Brown & Bildsten (1998). We assume that pure helium is accreting onto a NS and burning into heavier elements. It initially burns into ^{12}C via the triple- α process and then heavier elements (^{16}O , ^{20}Ne , ^{24}Mg , and ^{28}Si) via subsequent alpha captures. The envelope consists of three layers; a layer of pure accreted helium which is the “atmosphere,” a thin layer where the burning occurs, and a layer of heavy element ashes, the “ocean.” Below this is the rigid NS crust which will provide the bottom boundary for the modes.

2.1. Finding the Envelope Profile

We assume that the NS has a mass of $M = 1.4M_{\odot}$ and a radius of $R = 10$ km. Neglecting general relativity, the surface gravitational acceleration is then $g = GM/R^2 \approx 1.87 \times 10^{14}$ cm s $^{-2}$. The pressure scale height is $h = P/\rho g \approx 200$ cm at the burning layer. Since $h \ll R$ we assume that g is constant and that the envelope has plane-parallel geometry. This simplifies calculations of the envelope profile and the nonradial perturbations considered in §3. Hydrostatic balance then yields $P = gy$, where y is the column depth, $dy \equiv -\rho dr$, and r is the radial distance.

The plane-parallel nature of this problem implies that stability should depend on the accretion rate per unit area, \dot{m} (Fujimoto, Hanawa & Miyaji 1981; Fushiki & Lamb 1987b). We therefore parametrize the accretion in terms of the local Eddington rate per unit area for helium accretion (henceforth, simply referred to as the Eddington rate),

$$\dot{m}_{\text{Edd}} = \frac{2m_p c}{R\sigma_{\text{Th}}} = 1.5 \times 10^5 \text{ g cm}^{-2} \text{ s}^{-1} \left(\frac{10^6 \text{ cm}}{R} \right), \quad (1)$$

where m_p is the proton mass, c is the speed of light, and σ_{Th} is the Thomson cross section. NSs can accrete locally at rates higher than this if the accretion geometry allows radiation to escape without impeding the accretion flow. The flux within the atmosphere and ocean are still sub-Eddington because the potential energy of gravitational infall has been released long before material reaches these depths (where it is now in hydrostatic balance). We sometimes consider such super-Eddington rates because they are required for the thermal stability of the accreting envelope.

The continuity equation for an element i with mass fraction $X_i = \rho_i/\rho$ is

$$\frac{\partial X_i}{\partial t} + \dot{m} \frac{\partial X_i}{\partial y} = \frac{A_i m_p}{\rho} (-r_i^{\text{dest}} + r_i^{\text{prod}}), \quad (2)$$

where r_i^{dest} (r_i^{prod}) is the particle destruction (production) rate, A_i is the baryon number of species i , and $v = -\dot{m}/\rho$ is the downward flow velocity (Wallace, Woosley & Weaver 1982; Bildsten, Salpeter & Wasserman 1993). We assume steady state burning and set $\partial X_i/\partial t = 0$. For the triple- α reactions we use the energy generation rate from Fushiki & Lamb (1987a). At larger depths helium is burned in alpha captures to form heavier elements. For the $^{12}\text{C}(\alpha, \gamma)^{16}\text{O}$ reaction we use the reaction rate from Buchmann (1996, 1997) with the fitting formula that gives $S = 146$ keV barns at 300 keV center-of-mass energy. Caughlan & Fowler (1988) is used for all further reactions which includes $^{16}\text{O}(\alpha, \gamma)^{20}\text{Ne}$, $^{20}\text{Ne}(\alpha, \gamma)^{24}\text{Mg}$, and $^{24}\text{Mg}(\alpha, \gamma)^{28}\text{Si}$. Possible subsequent burning of silicon does not occur for the accretion rates we consider. We follow Schalbrock et al. (1983) and set the uncertainty factor in the $^{20}\text{Ne}(\alpha, \gamma)^{24}\text{Mg}$ and $^{24}\text{Mg}(\alpha, \gamma)^{28}\text{Si}$ reaction rates to 0.1, and screening is included following Salpeter & Van Horn (1969).

Since helium rich accreting material is most likely from a helium white dwarf companion of the NS, a more realistic model should include a fraction of ^{14}N in the composition. This is the most abundant heavy nucleus in the accreting material as this nucleus is the pile-up point during the catalytic CNO cycle in the progenitor of the helium white dwarf. Its abundance could be as large as 2%, and the only available fusion reaction in the accreting NS envelope is $^{14}\text{N}(\alpha, \gamma)^{18}\text{F}$, which releases 4.415 MeV. Using the rates from Caughlan & Fowler (1988) (also see Couch et al. 1972), we integrated the continuity equation for ^{14}N , finding that this element is quickly converted to ^{18}F at a shallow depth of 10^7 g cm $^{-2}$. Unless another α capture occurs, the ^{18}F will decay by positron emission to ^{18}O with a half-life of 109.8 minutes, creating a slight gradient in μ_e (the mean molecular weight per electron) in the envelope. By the time this decay occurs, all the α particles will have been consumed so that the usual closure of this chain to ^{22}Ne seems unlikely. This consumption of α particles is not dramatic enough to drastically affect the composition of other heavy α -capture elements, nor affect the temperature sensitivity of triple- α reactions which leads to instability of a mode. We therefore omit ^{14}N from our calculations. It is interesting to note that we do find a range of high accretion rates ($\dot{m} \sim 5\dot{m}_{\text{Edd}}$) where a thermal instability in the $^{14}\text{N}(\alpha, \gamma)^{18}\text{F}$ reaction will occur before triple- α in an accumulating envelope. The small amount of energy released in such unstable reactions would have little observational effect. An accreting pulsar such 4U 1626–67 might have the correct conditions for such a scenario to occur (if there is super-Eddington accretion occurring at its polar cap), but the flares that would be created by such unstable reactions (which would occur every ~ 100 s) would never exceed $\sim 10^{-3}$ of the accretion luminosity.

The entropy equation is

$$T \frac{ds}{dt} = -\frac{1}{\rho} \vec{\nabla} \cdot \vec{F} + \epsilon, \quad (3)$$

where s is the specific entropy (which has units of erg g $^{-1}$ K $^{-1}$), ϵ is the energy generation rate from nuclear reactions, and the flux leaving a plane-parallel atmosphere is given by the standard radiative transfer equation,

$$F = \frac{4acT^3}{3\kappa} \frac{dT}{dy}, \quad (4)$$

where κ is the opacity, and a is the radiation constant. Rewriting the specific entropy as a function of $T(y, t)$ and $P(y, t)$, equation (3) becomes

$$\frac{\partial F}{\partial y} + \epsilon = c_p \left(\frac{\partial T}{\partial t} + \dot{m} \frac{\partial T}{\partial y} \right) - \frac{c_p T \dot{m}}{y} \nabla_{ad}, \quad (5)$$

where c_p is the specific heat at constant pressure and $\nabla_{ad} \equiv (\partial \ln T / \partial \ln P)_s$. In steady state $\partial T / \partial t = 0$ so that

$$\frac{dF}{dy} = -\epsilon + c_p \dot{m} \left(\frac{\partial T}{\partial y} - \frac{T}{y} \nabla_{ad} \right), \quad (6)$$

where the last term is often referred to as gravitational compression.

Equations (2), (4), and (6) can now be solved numerically to find the structure of the envelope. We relate pressure and density using the analytic equations of state by Paczyński (1983b). The opacity in equation (4) is set by electron scattering, free-free, and conductive opacities. We use the electron scattering opacity as approximated in Paczyński (1983b). The free-free opacity is from Clayton (1983),

$$\kappa_{\text{ff}} = 0.753 \text{ cm}^2 \text{ g}^{-1} \frac{\rho_5}{T_8^{7/2}} \sum_i \frac{Z_i^2 X_i}{A_i} g_{\text{ff}}(Z_i, T, n_e), \quad (7)$$

where the sum is over all nuclear species, $\rho_5 = \rho / (10^5 \text{ g cm}^{-3})$, $T_8 = T / (10^8 \text{ K})$, Z_i is the charge of the nucleus of species i , and g_{ff} is the dimensionless Gaunt factor that is analytically fit in Schatz et al. (1999). This factor takes into account Coulomb wavefunction corrections, degeneracy, and relativistic effects. Free-free is never the dominant opacity, since when it becomes large the heat transport is mediated by conduction, but it must be included to correctly calculate the total opacity in the deeper regions of the envelope. The conductive opacity is from Schatz et al. (1999) which uses the basic form of Yakovlev & Urpin (1980).

Solving these equations requires setting boundary conditions for the flux and temperature. The flux exiting the envelope is the sum of the steady state nuclear burning flux, the internal gravitational energy release, and any additional flux coming from the crust, F_{crust} . The radiative zero nature of the outer boundary means that the surface temperature boundary condition is fairly simple (Schwarzschild 1958). Near the top of the envelope, where the flux is constant, hydrostatic balance can be combined with radiative diffusion, equation (4), to find $dP/dT \propto T^3/\kappa$. Integrating this result with the assumption that the opacity is nearly constant (electron scattering is the dominate opacity) provides the relation $P \propto T^4$ plus a constant of integration set by the initial value of the temperature. Since $T^4 \gg T_{\text{eff}}^4$ this constant is dwarfed at the depths of interest ($y \gtrsim 10^6 \text{ g cm}^{-2}$) making the initial choice of temperature negligible. Figure 1 shows nuclear compositions of envelopes as a function of column depth for different accretion rates and $F_{\text{crust}} = 0$. The helium mass fraction is depleted to $\approx 50\%$ near a column density of $5 \times 10^7 \text{ g cm}^{-2}$ (the burning layer). At high accretion rates, considerable amounts of heavy elements are formed in the deep ocean. Figure 2 shows the flux and temperature profiles for these same accretion rates. As the accretion rate increases, the temperature profile becomes hotter. Since these envelopes have no flux from the neutron star crust, the temperature is approximately isothermal (except from gravitational settling contributions) below the burning depth. In Figure 3, F_{crust} is increased

and the temperature profile becomes hotter and non-isothermal at large depths. In §3.3 we show how this extra flux alters the conditions for mode stability.

An important quantity when solving for the modes is the Brunt-Väisälä frequency (Bildsten & Cumming 1998),

$$N^2 = \frac{g}{h} \left\{ \frac{\chi_T}{\chi_\rho} \left[\nabla_{ad} - \left(\frac{d \ln T}{d \ln P} \right)_* \right] - \frac{\chi_{\mu_e}}{\chi_\rho} \left(\frac{d \ln \mu_e}{d \ln P} \right)_* - \frac{\chi_{\mu_i}}{\chi_\rho} \left(\frac{d \ln \mu_i}{d \ln P} \right)_* \right\}, \quad (8)$$

where $\chi_Q = \partial \ln P / \partial \ln Q$ with all other intensive variables set constant, and $*$ refers to derivatives of the envelope's profile. Figures 2 and 3 shows N versus accretion rate and base flux. The general profile of N is set by the increase in the scale height with depth because $N^2 \sim g/h$, but there is also a bump near the helium burning depth. This added buoyancy is caused by the change in the mean molecular weight as helium burns to carbon, and it has important consequences for the modes. At high accretion rates N shows additional structure due to the heavier elements that are being made, but this has little effect on the modes.

2.2. Applicability of Steady State Burning Models

It is important to understand when a steady state burning envelope will be thermally stable. One way is to have an envelope hot enough that the temperature sensitivity of triple- α reactions is weaker than that of cooling. This is easily accomplished at high accretion rates. A one-zone model approximates the competition between nuclear heating and radiative cooling in the helium burning layer. This argument (Fujimoto, Hanawa & Miyaji 1981) is reviewed in Bildsten (1998) and repeated here for completeness. For triple- α reactions we write $\epsilon_{3\alpha} \propto \rho^\eta T^\nu$. The cooling is set by the derivative of radiative transfer, equation (4), which in the one-zone approximation becomes

$$\frac{\partial F}{\partial y} \approx -\frac{acg^2 T^4}{3\kappa P^2} \equiv \epsilon_{\text{cool}}. \quad (9)$$

Comparing the temperature sensitivity of $\epsilon_{3\alpha}$ and ϵ_{cool} gives a local condition for stability as $d\epsilon_{3\alpha}/dT < -d\epsilon_{\text{cool}}/dT$. This can be written more explicitly in the steady state case ($\epsilon_{3\alpha} = -\epsilon_{\text{cool}}$) as

$$\nu - 4 + \frac{d \ln \kappa}{d \ln T} + \frac{d \ln \rho}{d \ln T} \left(\eta + \frac{d \ln \kappa}{d \ln \rho} \right) < 0. \quad (10)$$

Approximating $\nu = -3 + 44/T_8$, $\eta = 2$, $d \ln \kappa / d \ln T = 0$, $d \ln \kappa / d \ln \rho = 0$, and $d \ln \rho / d \ln T = -1$, we find $T > 4.8 \times 10^8 \text{ K}$ is needed for stable nuclear burning of pure helium. We then look at Figure 2 to find the corresponding accretion rate. From this we find that accretion must be at least 5–10 times the Eddington rate for stable burning.

Another way to suppress thermal instabilities is to have a large F_{crust} (Paczyński 1983a; Bildsten 1995). There is suggestive observational evidence of a lack of type I X-ray bursts in the days following a superburst (Cornelisse et al. 2000; Kuulkers et al. 2002) which may be due to the additional flux from cooling carbon ashes (as speculated in Cumming & Bildsten 2001). For these reasons we also study the mode structure for envelopes with high F_{crust} .

3. NONRADIAL OSCILLATIONS IN A THIN SHELL

Nonradial oscillations have been studied in detail for NSs both in isolation (McDermott, Van Horn & Scholl 1983; Finn 1987; McDermott, Van Horn & Hansen 1988; McDermott 1990; Reisenegger & Goldreich 1992; Strohmayer 1993) and accreting (McDermott & Taam 1987; Bildsten & Cutler 1995, hereafter BC95; Bildsten, Ushomirsky & Cutler 1996, hereafter BUC96; Strohmayer & Lee 1996; Bildsten & Cumming 1998). To solve the nonradial perturbations on a rotating neutron star we follow BUC96, but we also include additional new strategies that assist in solving these equations.

3.1. Adiabatic Perturbation Equations

In the outer envelope (at $y \approx 10^6 \text{ g cm}^{-2}$) the thermal timescale is $t_{\text{th}} \approx y c_p T / F \approx 0.1 \text{ sec}$. This will be shown to be shorter than the g-mode periods. This means we can consider purely adiabatic perturbations of as long as we confine our analysis to large enough depths ($y \gtrsim 10^6 \text{ g cm}^{-2}$). Damping will occur in those regions where the mode period is longer than the thermal time.

For the perturbations, we consider conservation of mass, $\partial \rho / \partial t + \vec{\nabla} \cdot (\rho \vec{v}) = 0$, and momentum,

$$\rho \left(\frac{\partial}{\partial t} + \vec{v} \cdot \vec{\nabla} \right) \vec{v} = -\vec{\nabla} P - \rho \vec{\nabla} \Phi - 2\vec{\Omega} \times \vec{v}, \quad (11)$$

where Φ is the gravitational potential, $\vec{\Omega}$ is the neutron star spin vector, and the last term is the Coriolis force. The centrifugal force can be neglected because $\Omega \ll (GM/R^3)^{1/2}$ for most accreting NSs (Chakrabarty et al. 2003). We make Eulerian perturbations of these conservation equations, substituting for the dependent variables $Q \rightarrow Q_0 + \delta Q$, where Q_0 denotes the static background (this subscript is dropped in subsequent expressions). Perturbations are assumed to have the form $\delta Q = \delta Q(r, \theta) \exp(im\phi + i\omega t)$ where ω is the mode frequency in the rotating frame (an observer will see a frequency $\omega_{\text{obs}} = |\omega - m\Omega|$). Since the background model has no fluid motion we substitute $\vec{v} \rightarrow \delta \vec{v} = d\vec{\xi}/dt$, where $\vec{\xi}$ is the local Lagrangian displacement. Keeping terms of linear order, continuity becomes

$$\delta \rho + \vec{\nabla} \cdot (\rho \vec{\xi}) = 0, \quad (12)$$

and the momentum equation can be broken into its three components to give

$$-\rho \omega^2 \xi_r = -\frac{\partial \delta P}{\partial r} - g \delta \rho + 2i\Omega \rho \omega \xi_\phi \sin \theta, \quad (13a)$$

$$-\rho \omega^2 \xi_\theta = -\frac{1}{R} \frac{\partial \delta P}{\partial \theta} + 2i\Omega \rho \omega \xi_\phi \cos \theta, \quad (13b)$$

$$-\rho \omega^2 \xi_\phi = -\frac{1}{R \sin \theta} \frac{\partial \delta P}{\partial \phi} - 2i\Omega \rho \omega (\xi_r \sin \theta + \xi_\theta \cos \theta). \quad (13c)$$

These equations can be further simplified using the ‘‘traditional approximation’’ (Chapman & Lindzen 1970; Brekhovskikh & Goncharov 1994; BUC96), allowing for separable solutions. The first simplification is neglecting the Coriolis force in equation (13a) for $\Omega \ll N^2 h / \omega R \sim 10^5 \text{ Hz}$. In the non-rotating case incompressibility tells us that $\xi_r / \xi_\theta \ll 1$ so we can also neglect the ξ_r term in equation (13c). Essentially we are assuming that the Coriolis force has no effect in the radial direction because of the strong gravitational field present and the thin size of the

envelope. In the adiabatic limit $\Delta P / P = \Delta \rho / (\Gamma_1 \rho)$, where Δ is a Lagrangian perturbation ($\Delta Q = \delta Q + \vec{\xi} \cdot \vec{\nabla} Q$) and Γ_1 is the adiabatic exponent, $\Gamma_1 \equiv (\partial \ln P / \partial \ln \rho)_s$. The radial equation then becomes identical to the non-rotating case,

$$\frac{d}{dr} \frac{\delta P}{P} = \left(1 - \frac{1}{\Gamma_1} \right) \frac{1}{h} \frac{\delta P}{P} + \left(\frac{\omega^2}{g} - \frac{N^2}{g} \right) \frac{\xi_r}{h}. \quad (14)$$

Combining equation (13b) with continuity, equation (12), results in

$$\frac{d\xi_r}{dr} = \frac{\xi_r}{\Gamma_1 h} - \frac{1}{\Gamma_1} \frac{\delta P}{P} - \frac{gh}{\omega^2 R^2} L_\mu \left[\frac{\delta P}{P} \right], \quad (15)$$

identical to the non-rotating result except now $-l(l+1)$ has been replaced by L_μ which is an angular operator, independent of the NS’s composition, defined as

$$L_\mu = \frac{\partial}{\partial \mu} \left[\frac{1 - \mu^2}{1 - q^2 \mu^2} \frac{\partial}{\partial \mu} \right] - \frac{m^2}{(1 - q^2 \mu^2)(1 - \mu^2)} - \frac{qm(1 + q^2 \mu^2)}{(1 - q^2 \mu^2)^2}, \quad (16)$$

where $q = 2\Omega/\omega$ and $\mu = \cos \theta$. The angular piece is now a separate eigenvalue equation,

$$L_\mu \left[\frac{\delta P}{P} \right] = -\lambda \frac{\delta P}{P}, \quad (17)$$

where λ is the ‘‘effective wavenumber’’ (BUC96).

We first focus on solving the radial eigenfunction equations in §3.2, and then return to solve for rotational modifications in §3.4 by solving for λ . In the limit that $\omega^2 \ll N^2$ (the limit for g-modes) it is easy to show that the frequency scales like $\omega \propto l(l+1)^{1/2}$, and therefore in the rotating case $\omega \propto \lambda^{1/2}$. We solve the radial structure for $l = 1$ with no rotation and define this frequency as ω_0 , later scaling to the rotationally modified frequency by setting $\omega = \omega_0(\lambda/2)^{1/2}$.

3.2. Solving the Radial Mode Structure

We now use equations (14) and (15) to solve for the radial eigenmode structure where we set $L_\mu[\delta P/P] = -l(l+1)\delta P/P$ and $l = 1$. In this section and §3.3, instead of considering ξ_r , ξ_θ , and ξ_ϕ we consider only ξ_r and ξ_\perp , where ξ_\perp is the vector displacement field perpendicular to ξ_r . We confine the radial structure to lie between $y \approx 10^6 \text{ g cm}^{-2}$ and $10^{13} \text{ g cm}^{-2}$. The top boundary (where we set $\Delta P = 0$) is set by our adiabatic approximation – we need to be at a sufficient depth so that the thermal time scale is longer than the mode period. In general this will be different for each mode and each envelope model, but it is always in the range of $10^5 - 10^6 \text{ g cm}^{-2}$ (see Appendix A of BC95 for how to deal with the transition to the outer atmosphere). The bottom boundary (where $\xi_r = 0$) is set at the crust where the material becomes rigid. Fortunately, the properties of the mode of most interest are nearly independent of this bottom boundary condition.

We numerically solve for the eigenfunctions, starting at the surface and shooting for the bottom boundary. As examples, we plot the first three g-modes with zero crossings (these will henceforth be referred to as the $n = 2, 3$, and 4 g-modes) in Figure 4 for an accretion rate of $5.0 \dot{m}_{\text{Edd}}$ and $F_{\text{crust}} = 0$. The perpendicular displacement is given by

$$|\xi_\perp| = \sqrt{l(l+1)} \frac{gh}{R\omega^2} \left| \frac{\delta P}{P} \right|. \quad (18)$$

The normalization is arbitrarily set to $\delta P/P = 1$ at the surface, but the ratio in sizes of ξ_r to ξ_\perp is meaningful and well approximated by the incompressible limit (which predicts $\xi_r/\xi_\perp \sim h/R$). Along with the radial and perpendicular displacements we include the logarithmic kinetic energy density of the modes

$$\frac{dE}{d \ln y} = \frac{1}{2} 4\pi R^2 \omega^2 |\xi_\perp|^2 y, \quad (19)$$

where we have used the approximation $\xi_r/\xi_\perp \sim h/R \ll 1$. This quantity shows where the mode “lives” in the envelope. The first mode in Figure 4 has a fairly constant ξ_\perp above the burning layer, and its amplitude falls off abruptly at larger depths. This mode, which we refer to as the “shallow surface wave,” resides primarily in the shallow helium layer above the carbon ash ocean and is fairly insensitive to the bottom boundary condition. This is also reflected by $dE/d \ln y$ which is small at the bottom of the ocean. On the other hand, the other modes in Figure 4, with a larger number of nodes, have energy densities that are nearly uniform as the frequency decreases. This shows that these modes will be sensitive to conditions at all depths including the bottom boundary.

The g-mode frequencies versus accretion rate are summarized in Figure 5. These approximately scale $\propto \dot{m}^{1/8}$ as we would expect from combining hydrostatics with radiative transfer and assuming $\omega^2 \sim ghk^2$, where $k^2 = l(l+1)/R^2$. The modes’ frequency dependence on F_{crust} is shown in Figure 6. The shallow surface wave ($n = 2$) changes the least as F_{crust} is changed because its energy density is confined above the ocean. All of the $l = 1$ frequencies are within the range of 10–30 Hz for a few nodes and decrease for higher order g-modes, as expected from WKB analysis.

3.3. Mode Stability

We now address the linear stability of these modes by considering the exchange of energy between the mode and the star. This involves calculating the “work integral” for each mode (Cox 1980; Unno et al. 1989). In the adiabatic non-rotating case that we considered in §3.1, equations (12) and (13) can be combined into one Hermitian operator, \mathcal{L} , acting on $\vec{\xi}$ which is

$$\begin{aligned} \mathcal{L}(\vec{\xi}) = & \frac{1}{\rho^2} (\vec{\nabla} P) \vec{\nabla} \cdot (\rho \vec{\xi}) \\ & - \frac{1}{\rho} \vec{\nabla} (\vec{\xi} \cdot \vec{\nabla} P) - \frac{1}{\rho} \vec{\nabla} (\Gamma_1 P \vec{\nabla} \cdot \vec{\xi}), \end{aligned} \quad (20)$$

where

$$\frac{d^2 \vec{\xi}}{dt^2} = -\mathcal{L}(\vec{\xi}) = -\omega^2 \vec{\xi}. \quad (21)$$

From this eigenvalue equation the clear interpretation of \mathcal{L} is that it gives the force per mass for a given vector displacement field $\vec{\xi}$. Since \mathcal{L} is Hermitian, we know that ω^2 must be purely real and therefore there are only damped or oscillatory solutions.

In the nonadiabatic case, the energy equation must also be included along with continuity and momentum conservation. This additional equation is written in the form

$$\frac{d \ln P}{dt} = \Gamma_1 \frac{d \ln \rho}{dt} + (\Gamma_3 - 1) \frac{\rho T}{P} \frac{ds}{dt}, \quad (22)$$

where Γ_3 is the adiabatic exponent, $\Gamma_3 - 1 \equiv (\partial \ln T / \partial \ln \rho)_s$. Taking perturbations and linearizing equation (22), followed by combining it with equations (12) and (13), the resulting expression can be manipulated to get

$$\begin{aligned} \frac{d}{dt} \left\{ \int_V \frac{1}{2} \rho \left| \frac{d\vec{\xi}}{dt} \right|^2 d\tau + \int_V \frac{1}{2} \vec{\xi} \cdot \mathcal{L}(\vec{\xi}) \rho d\tau \right\} \\ = - \int_V (\Gamma_3 - 1) T \Delta s \frac{d}{dt} \frac{\Delta \rho}{\rho} \rho d\tau. \end{aligned} \quad (23)$$

The first term on the left is the kinetic energy of the mode while the next term is the force dotted with the displacement, i.e. the work. We therefore identify the left hand side as the change in energy per unit time for the mode. The right hand side is then an equivalent expression for the change in energy. Averaging over one mode period and integrating by parts along with making the substitution

$$T \frac{d \Delta s}{dt} = \Delta \left(\epsilon - \frac{1}{\rho} \vec{\nabla} \cdot \vec{F} \right), \quad (24)$$

we obtain the the familiar work integral,

$$\left\langle \frac{d\Psi}{dt} \right\rangle = \frac{1}{\Pi} \int_0^\Pi dt \int_V (\Gamma_3 - 1) \frac{\Delta \rho}{\rho} \Delta \left(\epsilon - \frac{1}{\rho} \vec{\nabla} \cdot \vec{F} \right) \rho d\tau, \quad (25)$$

where Ψ is the mode energy, Π is the mode period, and $d\tau = 4\pi R^2 dr$ is a volume element. All perturbations are evaluated using an adiabatic eigenfunction so that this represents the first order imaginary correction to the mode frequency. If this integral is positive (negative) the mode will be excited (damped). It is important to note that just as for the thin shell thermonuclear instability, mode stability depends on a competition between heating (ϵ) and cooling ($\vec{\nabla} \cdot \vec{F} / \rho$). However, in the case of a mode, this difference is integrated over the entire envelope, weighted by the mode’s eigenfunction, giving a mathematically different stability criteria.

Figure 7 shows the logarithmic integrand from equation (25),

$$\text{Heating vs. Cooling} = (\Gamma_3 - 1) \frac{\Delta \rho}{\rho} \Delta \left(\epsilon - \frac{1}{\rho} \vec{\nabla} \cdot \vec{F} \right) y, \quad (26)$$

for three different modes at the same accretion rate. Regions where this function is positive (negative) show where the mode is being pumped (damped). It is clear that the $n = 2$ mode is excited while the others are damped. This excitation comes from an increase in nuclear reactions at the burning depth ($y \approx 5 \times 10^7 \text{ g cm}^{-2}$). By dividing the work integral by the integral of the energy density, equation (19), we derive an excitation rate,

$$\kappa_{\text{excite}} = \left\langle \frac{d\Psi}{dt} \right\rangle \left[\int \frac{dE}{d \ln y} d \ln y \right]^{-1}. \quad (27)$$

Figures 8 and 9 show this rate as a function of \dot{m} and F_{crust} and show that the excitation timescale can be as fast as less than a second for the shallow surface wave. All higher order g-modes are always damped ($\kappa_{\text{excite}} < 0$).

The work integrals calculated in this section are valid for all of the rotationally modified modes we consider in the next section, including the Kelvin modes and the r-modes. In the “traditional approximation” (§3.1) all of the inertial modes have

similar radial eigenfunctions because buoyancy dominates over the Coriolis force. The work integral only depends on the radial eigenfunction so that it will have the same value for each of the modes. The only differences between the rotationally modified modes' stabilities are their excitation rates. These depend on their kinetic energies, which are related to their frequencies, see equation (19). These frequencies are altered due to the Coriolis force as explained in the following section.

3.4. Solving the Angular Equation

We now discuss our methods for solving equation (17) that build on BUC96. This provides us with eigenfunctions that span the latitudinal length of the star and relates λ to q . Equation (17) is known as Laplace's tidal equation, and its solutions are Hough functions. For a standard method of how to solve this equation as an expansion of spherical harmonics for $q \sim 1$ see Longuet-Higgins (1968). However, since we are interested in large values of q (for which modes can decay exponentially towards the pole, requiring a large number of terms) we instead follow BUC96 and numerically solve this equation. The numerical challenges are singularities at $\mu = 1$ and $\mu = 1/q$ which were dealt with first in BUC96. An easier way to get around the singularity at $1/q$ is to break equation (17) into two first order differential equations.¹ We define $a \equiv \delta P/P$ and

$$b \equiv -\frac{1-\mu^2}{1-q^2\mu^2} \left[\frac{\partial a}{\partial \mu} - \frac{qm\mu}{1-\mu^2} a \right]. \quad (28)$$

Essentially we are setting $b \propto \sin\theta\xi_\theta$. Substituting these relations into Laplace's tidal equation results in two first order differential equations

$$(1-\mu^2) \frac{\partial a}{\partial \mu} = qm\mu a - (1-q^2\mu^2)b \quad (29)$$

$$\frac{\partial b}{\partial \mu} = \left(\lambda - \frac{m^2}{1-\mu^2} \right) a - \frac{qm\mu}{1-\mu^2} b. \quad (30)$$

These equations can be further simplified by factoring out the singularity at $\mu = 1$. This is done by defining $A \equiv (1-\mu^2)^{|m|/2} a$ and $B \equiv (1-\mu^2)^{|m|/2} b$ which provides the equations

$$(1-\mu^2) \frac{\partial A}{\partial \mu} = (|m|+qm)\mu A - (1-q^2\mu^2)B \quad (31)$$

$$\frac{\partial B}{\partial \mu} = \left(\lambda - \frac{m^2}{1-\mu^2} \right) A + \frac{(|m|-qm)\mu}{1-\mu^2} B. \quad (32)$$

In this new form the angular eigenvalue equation is fairly easy to solve.

We begin integration at $\mu = 1 - \epsilon$ (where ϵ is some small positive number), with the conditions that $A = 1$ and $B = (|m| + qm)\mu/(1 - q^2\mu^2)$ (the normalization of A is arbitrary because the equations are linear). The symmetry of the solutions allows us to shoot numerically toward $\mu = 0$, where the boundary condition is $A(0) = 0$ (for odd solutions) or $A'(0) = 0$ (for even solutions). The eigenvalues are tracked by starting at small q (little rotation) where $\lambda = l(l+1)$ and then increasing q while solving for the boundary condition at the equator.

Figure 10 shows the eigenvalues of the rotationally modified g-modes that correspond to $l = 1$ or $l = 2$ in the non-rotating limit as a function of q (as can be seen because $\lambda = 2$ or 6 for $q \ll 1$) (consistent with BUC96). In all cases, the lowest m

value mode for a given l has the interesting feature that at large q it asymptotes to $\lambda = m^2$. This is the ‘‘Kelvin mode’’ (Longuet-Higgins 1968). All other g-modes increase in λ for increasing q and asymptote to $\lambda \propto q^2$ (as discussed in Papaloizou & Pringle 1978 and BUC96).

Since the ‘‘traditional approximation’’ captures all rotationally modified modes of the star, we have also included in Figure 10 two of the odd parity r-modes (not shown in BUC96). These have the property that at small q there is a simple relationship between the neutron star spin and the mode frequency, namely $\omega = 2m\Omega/l(l+1)$ (Saio 1982; Lee & Saio 1986). At higher spin frequencies, the mode frequencies are shown to deviate from this relationship. Additional even and odd parity r-modes are shown in Figure 11. The r-modes all have $m > 0$ so they will move retrograde with respect to the neutron star spin. They would therefore appear below the spin frequency in observations (but not with the same spacing as the Kelvin mode).

Figure 12 shows some examples of the eigenfunctions that are found to span the latitudinal direction. It is important to note that for the rotationally modified g-modes, the eigenfunction becomes concentrated at the equator for higher spin rates. The modes are exponentially damped for $\mu \gtrsim 1/q$. On the other hand, other modes, such as the Kelvin mode, are not as affected by rotation and will have a larger amplitude covering a larger area of the surface.

4. OBSERVATIONAL TESTS

The closest physical realization of the model we describe in the previous sections is 4U 1820–30. This LMXB sits near the center of the globular cluster NGC 6624 and was the first to show type I X-ray bursts (Grindlay et al. 1976). It is also the LMXB with the shortest orbital period of 11.4 minutes (Stella, White & Priedhorsky 1987). Since the system is so compact, the donor star is most likely a $0.06 - 0.08 M_\odot$ helium white dwarf (Rappaport et al. 1987) which means that the accreted material is very helium rich. This is consistent with the cooling timescale of X-ray bursts (10–20 seconds) and the photospheric radius expansions seen from this source (for examples, see Haberl et al. 1987).

4U 1820–30 has a 171.033 ± 0.326 day modulation between high and low luminosity states (Priedhorsky & Terrell 1984; Chou & Grindlay 2001). X-ray bursts are only seen during the low-luminosity state (Clark et al. 1977; Stella, Kahn & Grindlay 1984) which suggests that these modulations are related to the accretion rate. Such a scenario is qualitatively consistent with our understanding of thermal instabilities as discussed in §2.2. During the low state the bursting properties, including fluences and recurrence times, are well understood using current bursting models (Cumming 2003). An outstanding problem still remains in understanding the high-luminosity state because bursting is suppressed even though 4U 1820–30 is still well below the Eddington rate. This might be related to a change in the physics of the bursts from being convective to radiative in the high state (Bildsten 1995). 4U 1820–30 has also shown a ~ 3 hour long thermonuclear burst (Strohmayer & Brown 2001), or superburst, which is likely from unstable carbon burning. Other LMXBs such as 4U 1735–44 and GX 17+2 show that type I bursting ceases for many days following a superburst (Cornelisse et al. 2000; Kuulkers et al. 2002) which has been hypothesized to be due to additional flux due to cooling carbon ashes (Cumming & Bildsten 2001).

¹We thank Phil Arras and Greg Ushomirsky for pointing out this simplification.

As was shown in §3.4, the mode frequencies can become highly modified for the high spin rates (200–700 Hz) inferred from accreting X-ray pulsars and X-ray burst oscillations (Chakrabarty et al. 2003). However, 4U 1820–30 has never shown burst oscillations and therefore has an unknown spin period. Thankfully, we only have one unstable mode to consider, so we show how its frequency is modified as a function of the spin rate in Figure 13. By measuring multiple frequencies from 4U 1820–30 during one of its non-bursting states one could hope to constrain its spin period. In Figure 14 we show a similar plot focusing on the most probable spin rates for 4U 1820–30.

The lack of pulsations from most LMXBs implies a low magnetic field. This is helpful for the mode calculations as a large magnetic field would resist shearing from the change in ξ_{\perp} and modify the mode frequency. Following BC95, we estimate the maximum magnetic field before the shallow surface mode would be dynamically effected as $B_{\text{dyn}}^2 \approx 8\pi h^2 \rho \omega^2$, resulting in

$$B_{\text{dyn}} \approx 5 \times 10^7 \text{ G} \left(\frac{\omega/(2\pi)}{21.4 \text{ Hz}} \right). \quad (33)$$

For the case of Kelvin or r-modes B_{dyn} is constrained to be even smaller because these modes have smaller frequencies in the rotating frame.

Unfortunately, neither 4U 1820–30, nor any other helium accreting LMXBs (such as the recently detected ultracompacts in outburst though they have even lower accretion rates), has ever shown oscillations like the ones we describe. This may not be surprising since during high accretion states one might expect the surface of the neutron star to be obscured by material that cannot make its way to the surface due to radiation pressure. Furthermore, the rotationally modified eigenfunctions are squeezed toward the equator (as shown in Figure 12) meaning that modes may be covered by the accretion disk. We hope that by constraining the possible frequencies at which modes could occur, and noting that mode excitation is best when burning is steady, that searches for the modes will now be easier.

This study also brings to light the importance that a shallow surface wave might play for NSs. There are many other NS envelopes that have the properties that this mode needs to exist – namely a density or mean molecular weight discontinuity. In the short time (\sim seconds) after a type I X-ray burst, the NS envelope is composed of a hot, low density, layer of hydrogen and helium sitting on top of a high density layer of heavy nuclei ashes. In this case the discontinuity is even more extreme than the case we consider because of the presence of hydrogen and the heavy rapid proton capture elements in the ocean (Wallace & Woosely 1981; Hanawa, Sugimoto & Hashimoto 1983; Wallace & Woosely 1984; Schatz et al. 1997, 1998; Koike et al. 1999). Furthermore, if ignition of the type I X-ray burst were non-axisymmetric it could drive modes such as these. Even though we have not evaluated the stability, it seems likely that a shallow surface wave would exist in such circumstances. Previous theoretical studies predict static frequencies (for example McDermott & Taam 1987; Strohmayer & Lee 1996), but due to the temperature dependence of the shallow surface wave ($\omega \propto T^{1/2}$) it would be shifting in frequency and possibly not seen easily in a standard Fourier analysis. A frequency scan (with changing ω) would likely make these modes easier to find. We will discuss the sign and sizes of these frequency shifts, related to the NS temperature and spin, in a future paper.

5. CONCLUSIONS AND DISCUSSION

This study makes clear the distinction between thermal and mode perturbations of the thin envelope of a NS. We find one excited mode on a thermally stable helium accreting NS which is a shallow surface wave riding in the helium atmosphere above the ash ocean. It has a frequency of $(20 - 30 \text{ Hz})(l(l+1)/2)^{1/2}$ (depending on the accretion rate) and has an excitation time of about a second. This mode is modified by rotation to give multiple possible observable frequencies. Seeing such a frequency pattern from a NS could be used to constrain properties of the NS star (e.g. its spin or radius). The rotationally modified eigenfunctions will have different levels of visibility depending on both their final amplitudes and their angular eigenvalues. The LMXB 4U 1820–30 is accreting helium rich material and is the best candidate for having an envelope like the ones we consider. No such oscillations have yet been reported from it, but perhaps now that predictions have been made, a search for modes would be easier, especially when bursting is absent. Making comparisons with just this one system is limited, and it would be useful to do a similar mode stability analysis on NSs that are accreting a solar mix of hydrogen and helium, especially during times following a superburst when type I bursts are not occurring.

A further study could also address the eventual nonlinear evolution of the excited mode. Such a study might predict observational effects that this mode may exhibit. If this mode were to saturate at a low amplitude (as is common in most other stars) then the most observable feature would be the periodic modulation of the surface luminosity. If the mode saturation is the result of mode coupling, then other frequencies might also be visible. If the amplitude becomes exceedingly nonlinear, the resulting large temperature excursions may well lead to a more rapid consumption of the fuel than the rate of supply, possibly triggering limit cycle behavior.

This study highlights the importance a shallow surface wave may play on NSs, and we plan to continue an investigation to understand better what other NS environments might show this mode. An interesting study would be the time before or after type I X-ray bursts when the NS envelope should have the mean molecular weight discontinuity necessary to exhibit this mode. In the latter case the frequency of the mode would be changing due to the cooling of the atmosphere. This implies that shifting frequency searches may be the correct way to find these modes. A future paper will consider such effects in more detail, including the size and sign of the expected shifts.

Above all, this study has shown that spherically symmetric studies are not complete and can easily miss important physics that may be relevant for correctly understanding the properties of NSs. We hope to extend our work to type I X-ray burst ignition, which has not been fully investigated in the non-axisymmetric case. It is still somewhat unsatisfactory to think that a NS ignites spherically all at once, and our study makes clear that nonradial perturbations may give different stability criterion for ignition than what has commonly been used.

We thank Andrew Cumming for some of the original inspiration for beginning this research and Phil Arras for discussions concerning g-modes and rotational modifications. We have benefited greatly from conversations with Philip Chang, Chris Deloye, Aristotle Socrates, Anatoly Spitkovsky, Ronald Taam, Dean Townsley, and Greg Ushomirsky. We thank the anonymous referee for suggestions which have added clarity to this manuscript. This work was supported by the National

Science Foundation under grants PHY99-07949 and AST02-05956 and by NASA through grant NAG 5-8658. L. B. is a

Cottrell Scholar of the Research Corporation.

REFERENCES

- Bildsten, L. 1995, *ApJ*, 438, 852
 Bildsten, L. 1998, in *The Many Faces of Neutron Stars*, ed. R. Buccheri, J. van Paradijs & A. Alpar (Dordrecht: Kluwer), p. 419
 Bildsten, L. & Cumming, A. 1998, *ApJ*, 506, 842
 Bildsten, L. & Cutler, C. 1995, *ApJ*, 449, 800 (BC95)
 Bildsten, L., Salpeter, E. E. & Wasserman, I. 1993, *ApJ*, 408, 615
 Bildsten, L., Ushomirsky, G. & Cutler, C. 1996, *ApJ*, 460, 827 (BUC96)
 Brekhovskikh, L. M. & Goncharov, V. 1994, *Mechanics of Continua and Wave Dynamics* (Berlin: Springer)
 Brown, E. F. & Bildsten, L. 1998, *ApJ*, 496, 915
 Buchmann, L. 1996, *ApJ*, 468, L127
 Buchmann, L. 1997, *ApJ*, 479, L153
 Caughlan, G. R. & Fowler, W. A. 1988, *At. Data Nucl. Data Tables*, 40, 283
 Chakrabarty, D. et al. 2003, *Nature*, 424, 42
 Chapman, S. & Lindzen, R. S. 1970, *Atmospheric Tides* (Dordrecht: Reidel)
 Chou, Y. & Grindlay, J. E. 2001, *ApJ*, 563, 934
 Clark, G. W., Jernigan, J. G., Bradt, H., Canizares, C., Lewin, W. H. G., Li, F. K., Mayer, W., McClintock, J. & Schnopper, H. 1976, *ApJ*, 207, L105
 Clayton, D. D. 1983, *Principles of Stellar Evolution and Nucleosynthesis* (Chicago: Univ. Chicago Press)
 Cornelisse, R., Heise, J., Kuulkers, E., Verbrunt, F. & in 't Zand, J. J. M. 2000 *A&A*, 357, L21
 Couch, R. G., Spinka, H., Tombrello, T. A. & Weaver, T. A. 1972, *ApJ*, 172, 395
 Cox, J. P. 1980, *Theory of Stellar Pulsation* (Princeton: Princeton Univ. Press)
 Cumming, A. 2003, *ApJ*, 595, 1077
 Finn, L. S. 1987, *MNRAS*, 227, 265
 Fujimoto, M. Y., Hanawa, T. & Miyaji, S. 1981, *ApJ*, 247, 267
 Fushiki, I. & Lamb, D. Q. 1987a, *ApJ*, 317, 368
 Fushiki, I. & Lamb, D. Q. 1987b, *ApJ*, 323, L55
 Grindlay, J. E., Gursky, H., Schnopper, H., Parsignault, D. R., Heise, J., Brinkman, A. C. & Schrijver, J. 1976, *ApJ*, 205, L127
 Haberl, F., Stella, L., White, N. E., Priedhorsky, W. C. & Gottwald, M. 1987, *ApJ*, 314, 266
 Hanawa, T., Sugimoto, D. & Hashimoto, M. 1983 *PASJ*, 35, 491
 Hansen, C. J. & Van Horn, H. M. 1975, *ApJ*, 195, 735
 Joss, P. C. 1977, *Nature*, 270, 310
 Koike, O., Hashimoto, M., Arai, K. & Wanajo, S. 1999, *A&A*, 342, 464
 Kuulkers, E., Homan, J., van der Klis, M. Lewin, W. H. G. & Mèndez, M. 2002, *A&A*, 382, 947
 Lamb, D. Q. & Lamb, F. K. 1978, *ApJ*, 220, 291
 Lee, U. & Saio, H. 1986, *MNRAS*, 221, 365
 Longuet-Higgins, M. S. 1968, *Phil. Trans. R. Soc. London*, 262, 511
 Maraschi, L. & Cavaliere, A. 1977, *Highlights Astron.* 4, 127
 McDermott, P. N. 1990, *MNRAS*, 245, 508
 McDermott, P. N. & Taam, R. E. 1987, *ApJ*, 318, 278
 McDermott, P. N., Van Horn, H. M. & Hansen, C. J. 1988, *ApJ*, 325, 725
 McDermott, P. N., Van Horn, H. M. & Scholl, J. F. 1983, *ApJ*, 268, 837
 Narayan, R. & Heyl J. S., 2003, *ApJ*, in press (astro-ph/0303447)
 Paczyński, B. 1983a, *ApJ*, 264, 282
 Paczyński, B. 1983b, *ApJ*, 267, 315
 Papaloizou, J. & Pringle, J. E. 1978, *MNRAS*, 182, 423
 Priedhorsky, W. & Terrell, J. 1984, *ApJ*, 284, L17
 Rappaport, S., Ma, C. P., Joss, P. C. & Nelson, L. A. 1987, *ApJ*, 322, 842
 Reisneger, A. & Goldreich, P. 1992, *ApJ*, 395, 240
 Saio, H. 1982, *ApJ*, 256, 717
 Salpeter, E. E. & Van Horn, H. M. 1969, *ApJ*, 155, 183
 Schatz, H., Bildsten, L., Cumming, A. & Wiescher, M. 1999, *ApJ*, 524, 1014
 Schatz, H., Bildsten, L., Gorres, J., Wiescher, M. & Thielemann, F.-K. 1997, in *AIP Conf. Proc. 412, Intersections Between Particle and Nuclear Physics*, ed. T. W. Donnelly (New York: AIP), p. 987
 Schatz, H. et al. 1998, *Phys. Rep.*, 294, 167
 Schmalbrock, P., et al. 1983, *Nucl. Phys. A*, 398, 279
 Schwarzschild, M. 1958, *Structure and Evolution of the Stars* (New York: Dover Publications)
 Schwarzschild, M. & Härm, R. 1965, *ApJ*, 142, 855
 Stella, L., Kahn, S. M. & Grindlay, J. E. 1984, *ApJ*, 282, 713
 Stella, L., White, N. E. & Priedhorsky, W. 1987, *ApJ*, 312, L17
 Strohmayer, T. E. 1993, *ApJ*, 417, 273
 Strohmayer, T. E. & Bildsten, L. 2003 to appear in *Compact Stellar X-Ray Sources*, ed. W.H.G. Lewin and M. van der Klis, Cambridge University Press (astro-ph/0301544)
 Strohmayer, T. E. & Brown, E. F. 2001, *ApJ*, 566, 1045
 Strohmayer, T. E. & Lee, U. 1996, *ApJ*, 467, 773
 Unno, W., Osaki, Y., Ando, H., Saio, H. & Shibahashi, H. 1988, *Nonradial Oscillations of Stars* (Tokyo: Univ. Tokyo Press)
 Wallace, R. K. & Woosley, S. E. 1981, *ApJS*, 45, 389
 Wallace, R. K. & Woosley, S. E. 1984, in *AIP Conf. Proc. 115, High-Energy Transients in Astrophysics*, ed. S. E. Woosley (New York: AIP), 319
 Wallace, R. K., Woosley, S. E. & Weaver, T. A. 1982, *ApJ*, 258, 696
 Woosley, S. E. & Taam, R. E. 1976, *Nature*, 263, 101
 Woosley, S. E., et al. 2003, *ApJ*, submitted (astro-ph/0307425)
 Yakovlev, D. G. & Urpin, V. A. 1980, *Soviet Astron.*, 24, 303

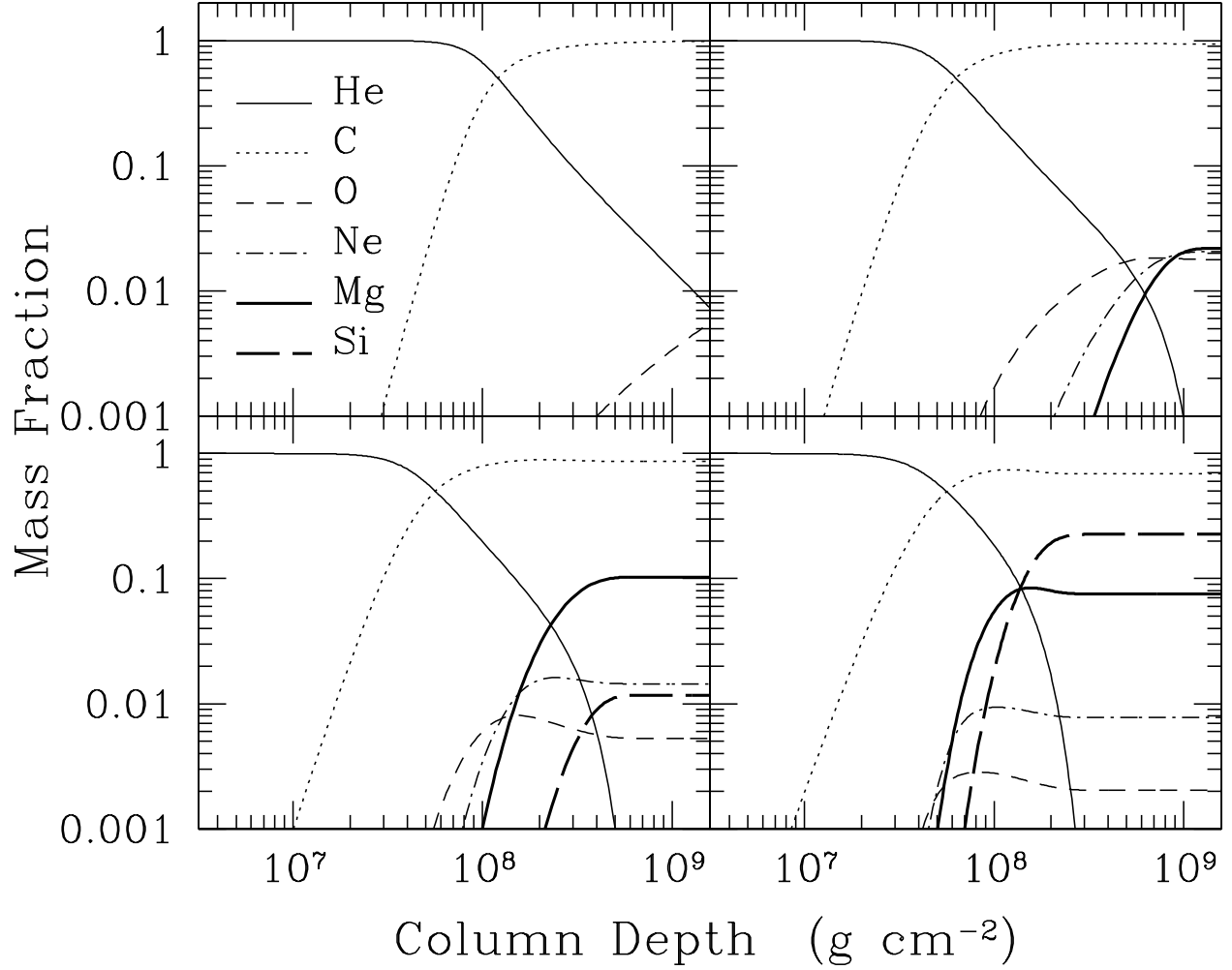


FIG. 1.— The composition of a neutron star envelope undergoing pure helium accretion and burning in steady state. The accretion rates are 1.0, 5.0, 10.0, and 20.0 (in units of $\dot{m}_{\text{Edd}} = 1.5 \times 10^5 \text{ g cm}^{-2} \text{ s}^{-1}$), starting at the upper left and going clockwise, all with $F_{\text{crust}} = 0$.

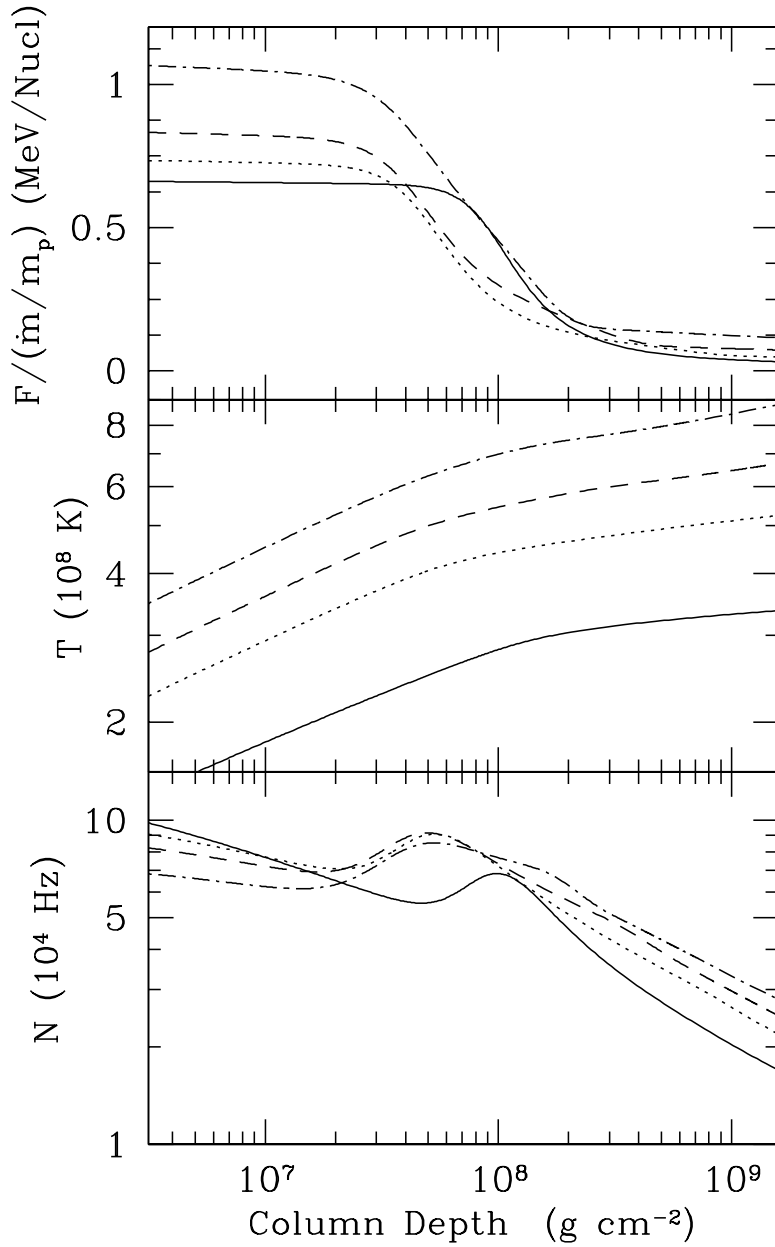


FIG. 2.— The flux per accreted nucleon (in units of MeV per nucleon), temperature, and Brunt-Väisälä frequency, N , for a neutron star undergoing pure helium accretion and burning in steady state. This figure shows accretion rates of 1.0 (solid line), 5.0 (dotted line), 10.0 (dashed line), and 20.0 (dot-dashed line) (in units of \dot{m}_{Edd}), all with $F_{\text{crust}} = 0$ (at a column density of 10^{13} g cm⁻²). The Brunt-Väisälä frequency shows a slight bump near the burning layer due to additional buoyancy provided by the change in mean molecular weight as helium burns to carbon.

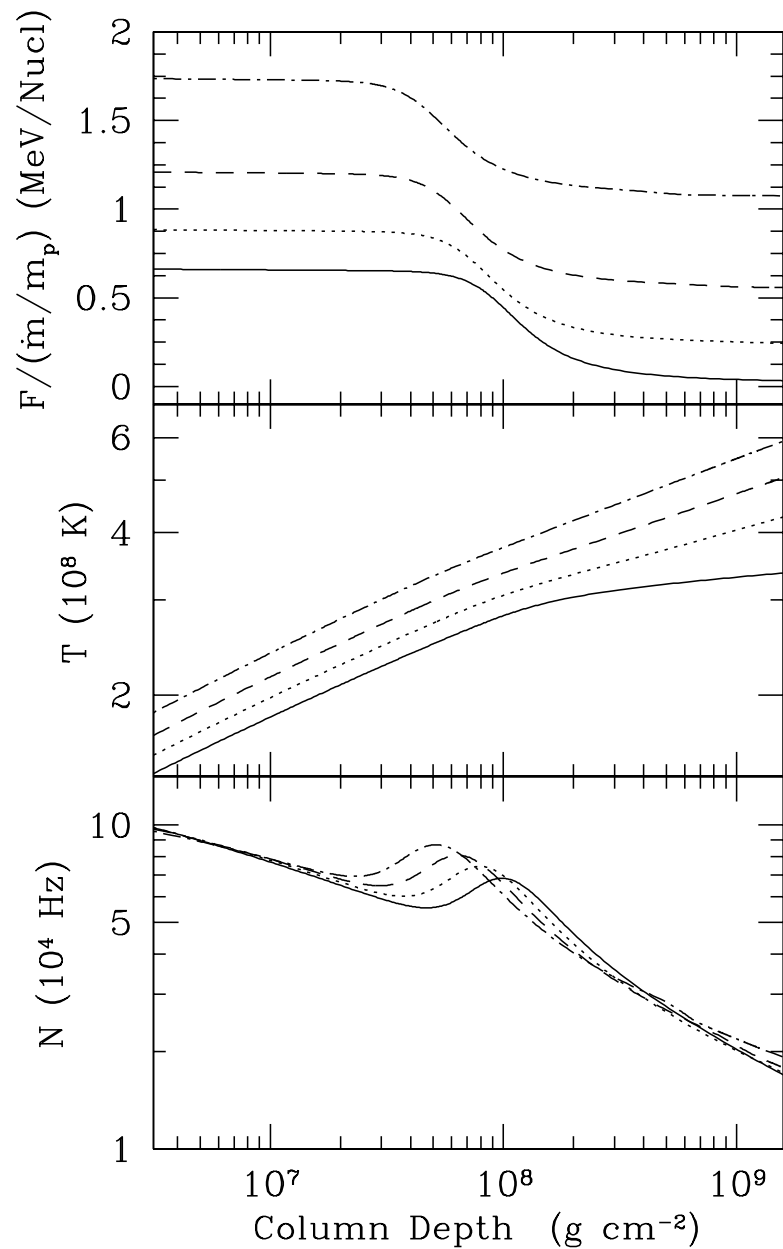


FIG. 3.— Same as Figure 2, but with F_{crust} values of 0.0 (solid line), 0.2 (dotted line), 0.5 (dashed line), and 1.0 (dot-dashed line) (in units of MeV per accreted nucleon), all with $\dot{m} = \dot{m}_{\text{Edd}}$.

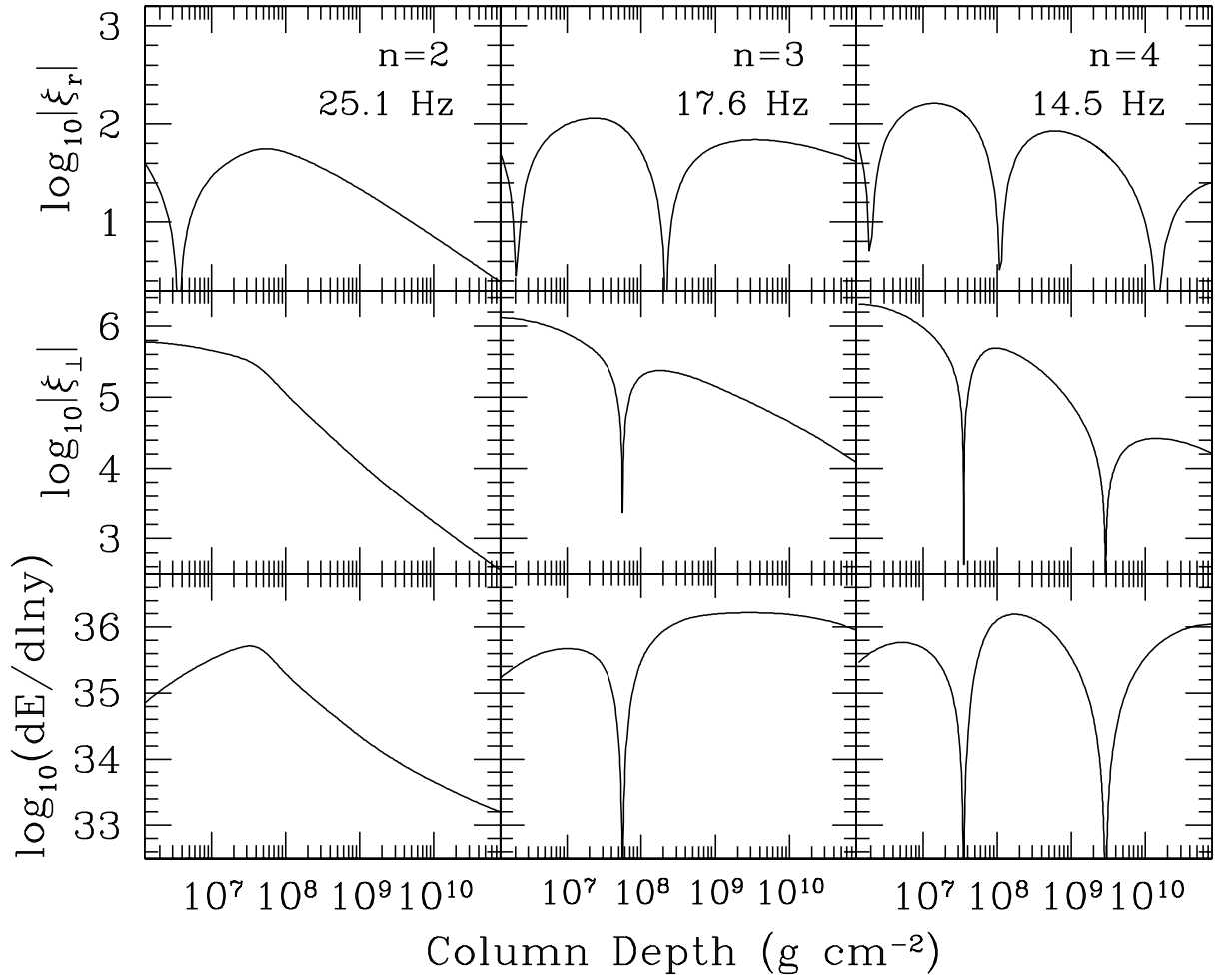


FIG. 4.— The radial eigenfunctions for the first three g-modes (with zero crossings in ξ_r) on a $\dot{m} = 5\dot{m}_{\text{Edd}}$, $F_{\text{crust}} = 0$ accreting neutron star envelope. The top (middle) panel shows the absolute displacement of the mode amplitude ξ_r (ξ_{\perp}) in units of cm. The normalization is arbitrary, but the relative amplitudes are significant. The cusps are zero crossings where the amplitude changes sign. The bottom panel shows the logarithmic energy density in units of ergs.

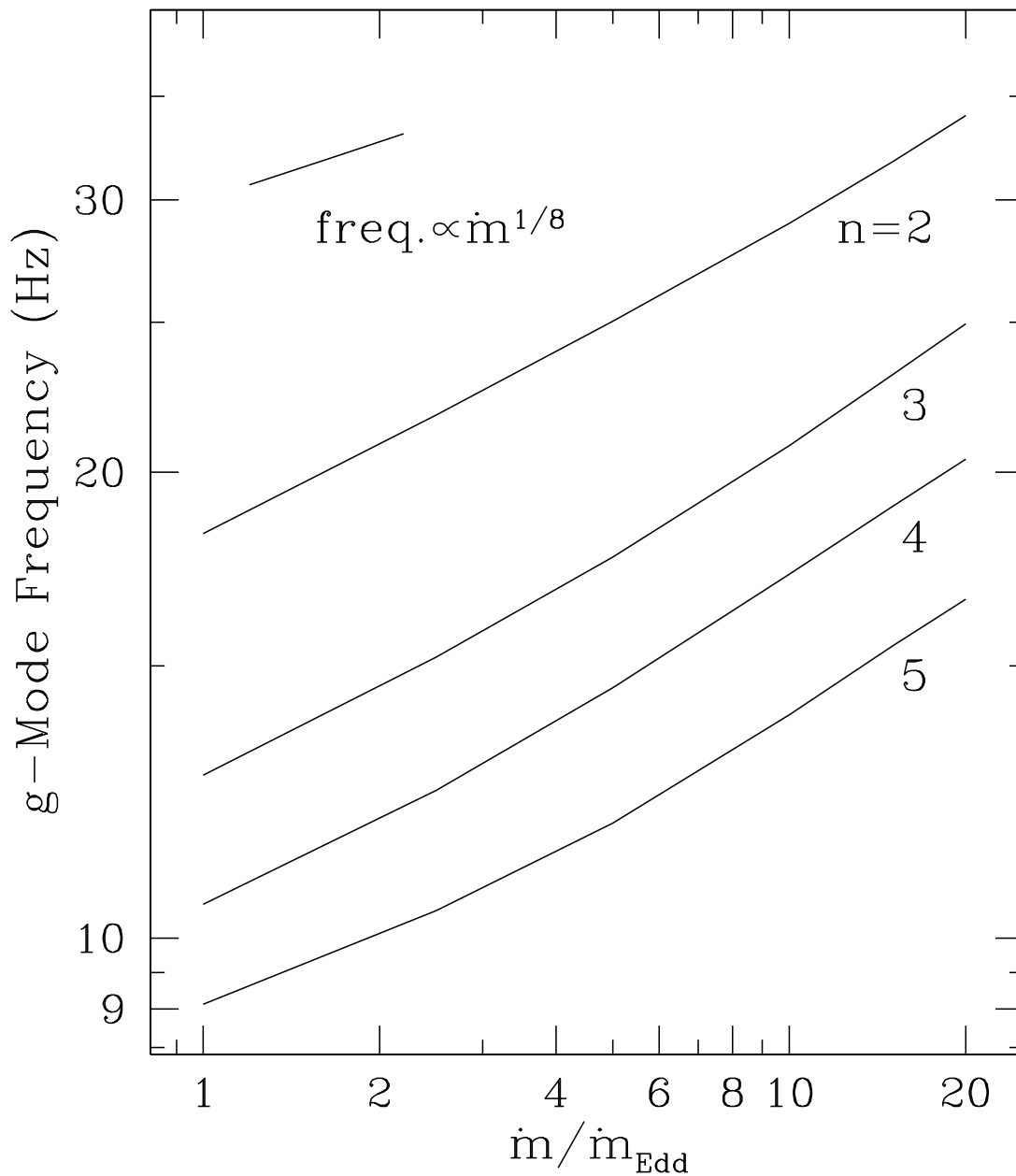


FIG. 5.— The g-mode frequencies for a non-rotating neutron star as a function of the accretion rate and for $l = 1$ ($F_{\text{crust}} = 0$). The frequency scales approximately $\propto \dot{m}^{1/8}$ as would be expected from a simple analytical analysis of the mode frequency.

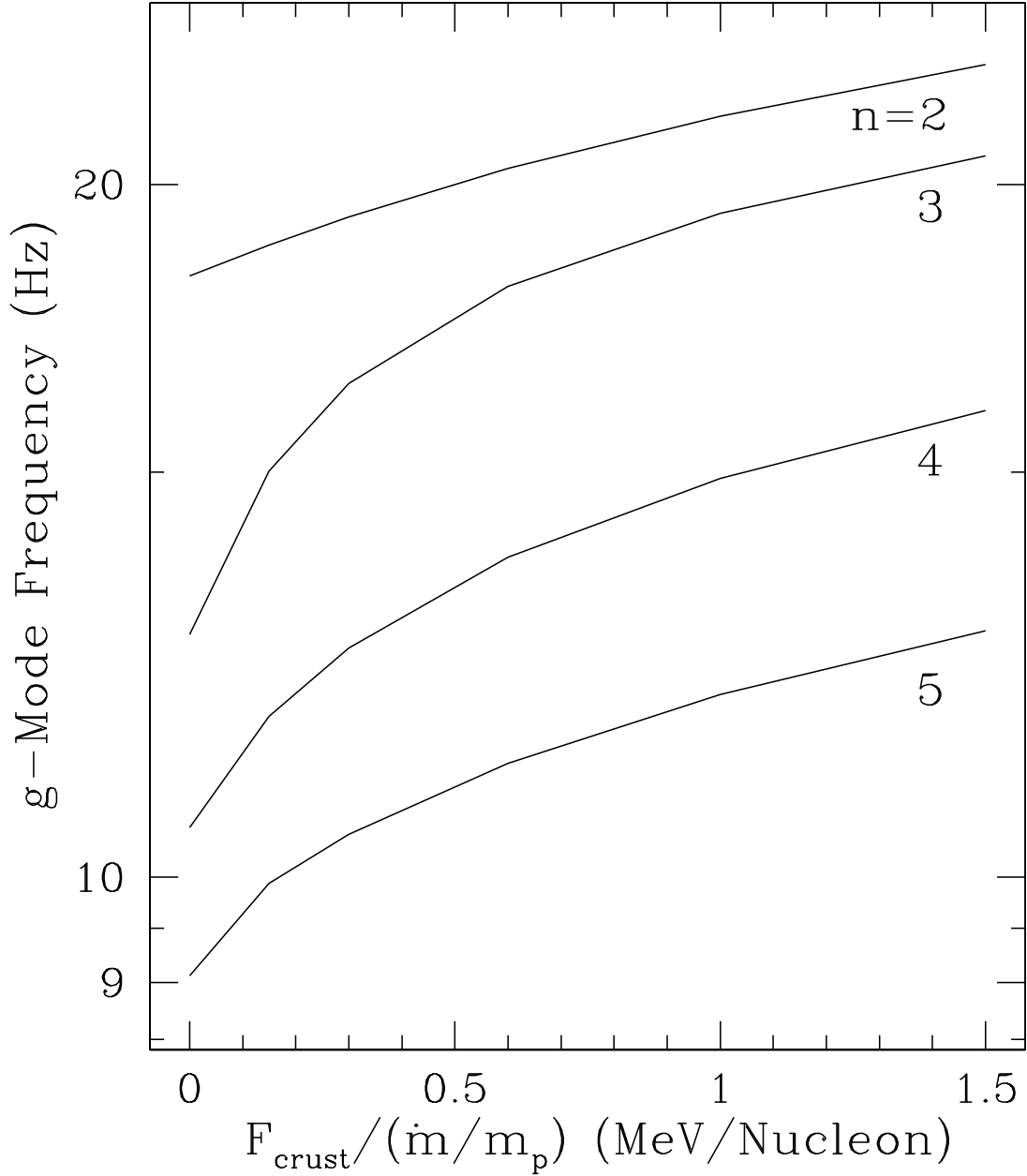


FIG. 6.— Same as Figure 5, but as a function of F_{crust} instead ($\dot{m} = \dot{m}_{\text{Edd}}$). The shallow surface wave ($n = 2$) frequency does not show the same degree of dependence on this change of the bottom boundary conditions.

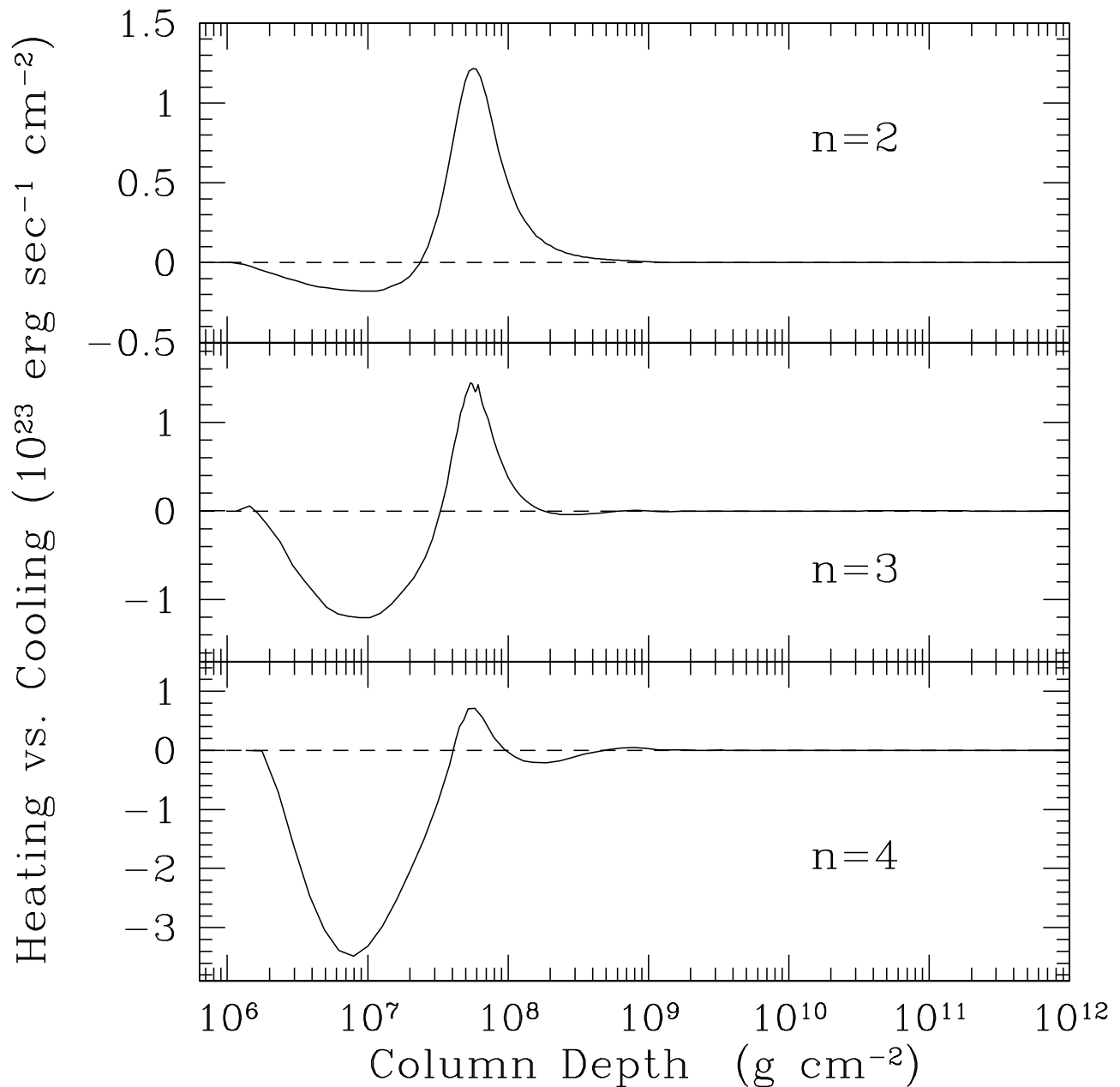


FIG. 7.— The logarithmic work integral integrand, equation (26), for three different modes. Regions above zero are pumping the mode while regions below zero are damping the mode. The majority of the pumping is due to increases in nuclear burning near the burning layer ($y \approx 5 \times 10^7 \text{ g cm}^{-2}$), while most of the radiative damping happens near the surface. The integrand necessarily goes to zero at the outer boundary condition (where $\Pi = t_{\text{th}}$) because $\Delta P/P = 0$. From this figure it is clear that the shallow surface wave ($n = 2$) is excited while the others are damped.

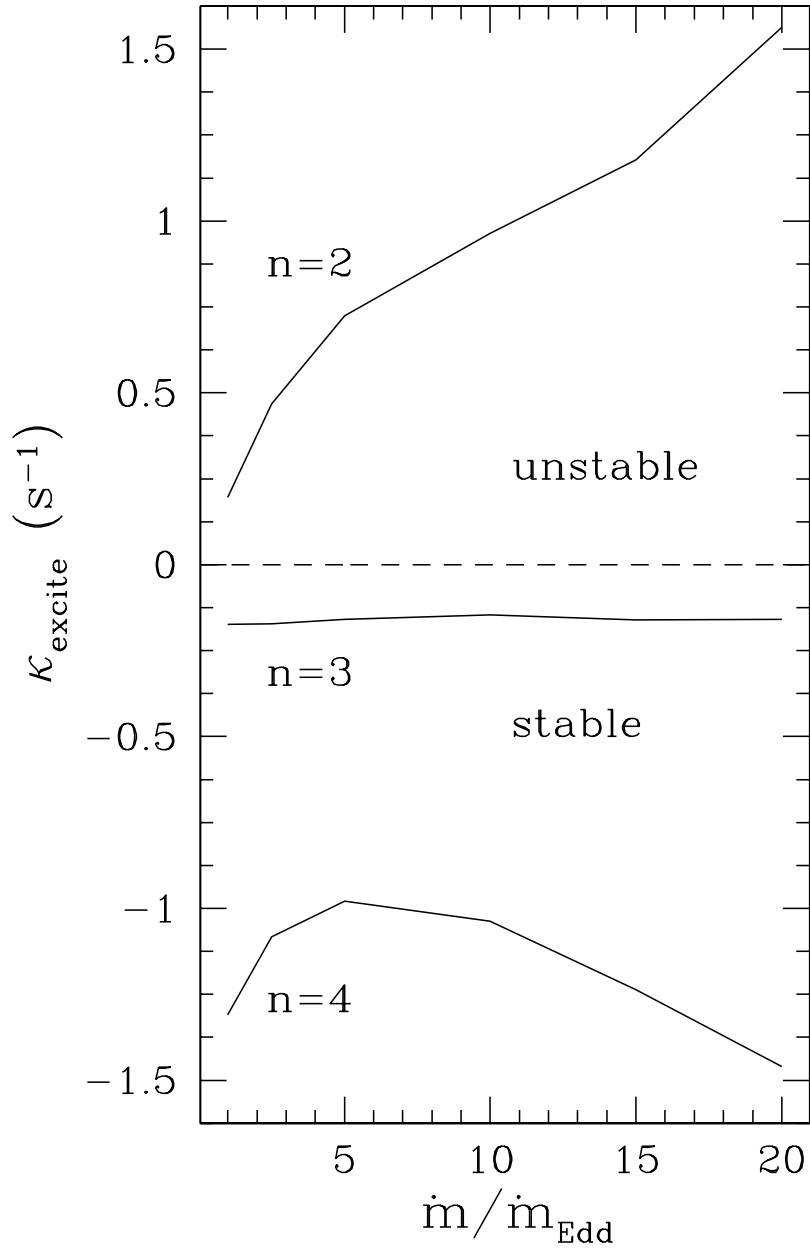


FIG. 8.— The excitation or damping rate due to nonadiabatic effects as a function of accretion rate. The inverse of κ_{excite} is the excitation (or damping) time. The shallow surface wave ($n = 2$) is excited more rapidly as \dot{m} increases while all higher order g-modes are damped.

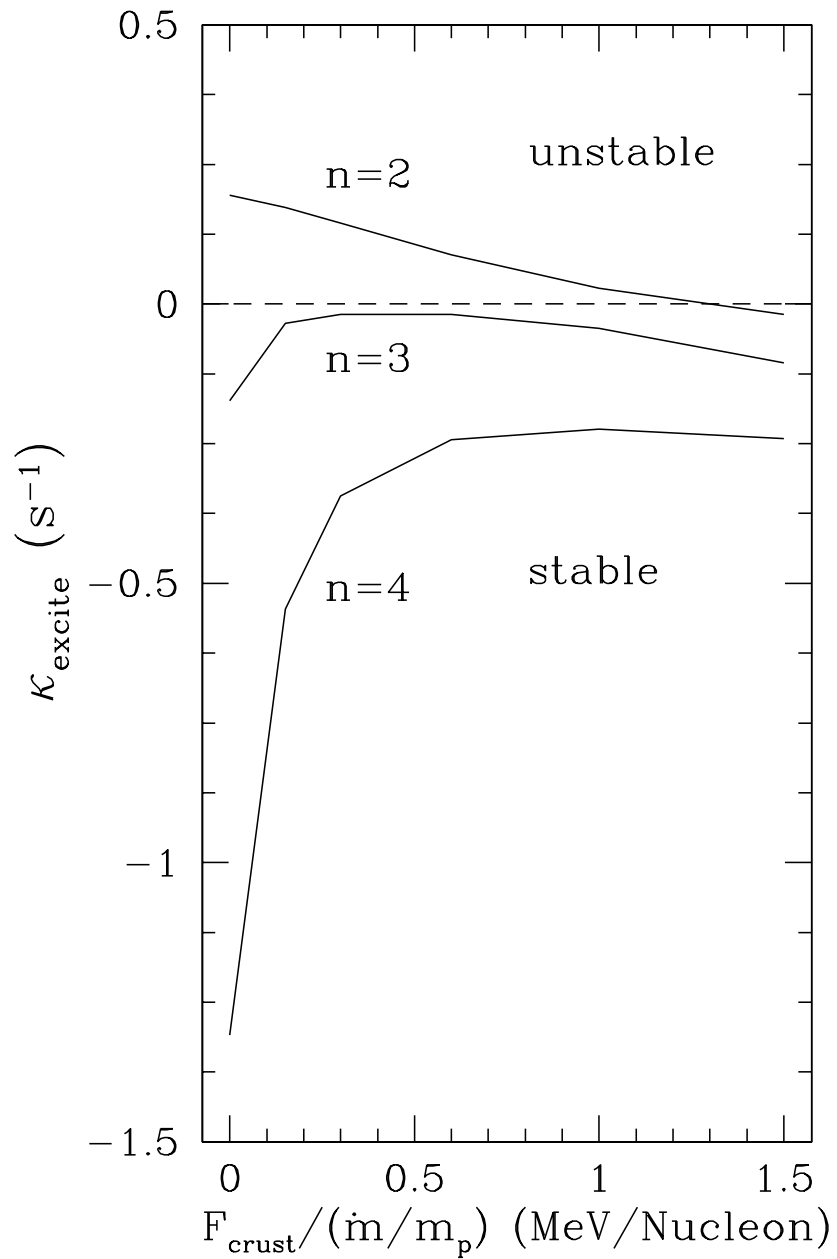


FIG. 9.— Same as Figure 8, but as a function of F_{crust} instead ($\dot{m} = \dot{m}_{\text{Edd}}$). As F_{crust} increases, eventually even the shallow surface wave is damped ($F_{\text{crust}} \approx 1.3 \text{ MeV/Nucleon}$).

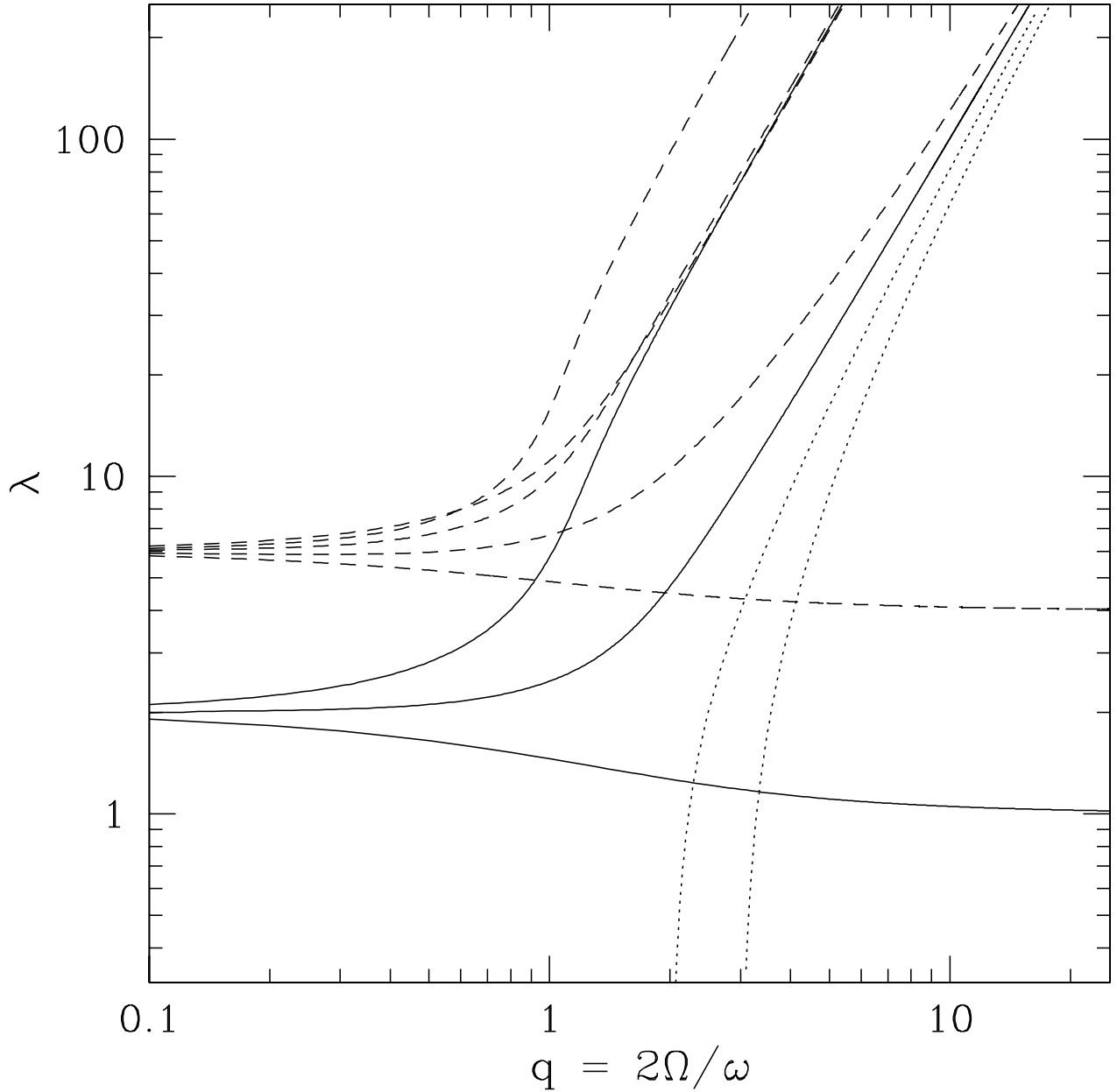


FIG. 10.— The effective wavenumber, λ , for modes on a rotating star versus the quantity $q = 2\Omega/\omega$. Solid lines denote modes for which $l = 1$ in the non-rotating limit with m values of $-1, 0$, and 1 (from bottom to top). The dashed lines denote modes for which $l = 2$ in the non-rotating limit with m values $-2, -1, 0, 1$, and 2 (from bottom to top). For $q \ll 1$, $\lambda \approx l(l+1)$. For $q \gg 1$, $\lambda \propto q^2$, except for the lowest m mode which goes to $\lambda = m^2$ (the Kelvin mode). The dotted lines denote two of the odd parity r-modes (from left to right, $l = 1, m = 1$ and $l = 2, m = 2$) which satisfy $\omega = 2m\Omega/l(l+1)$ in the $\lambda \ll 1$ limit.

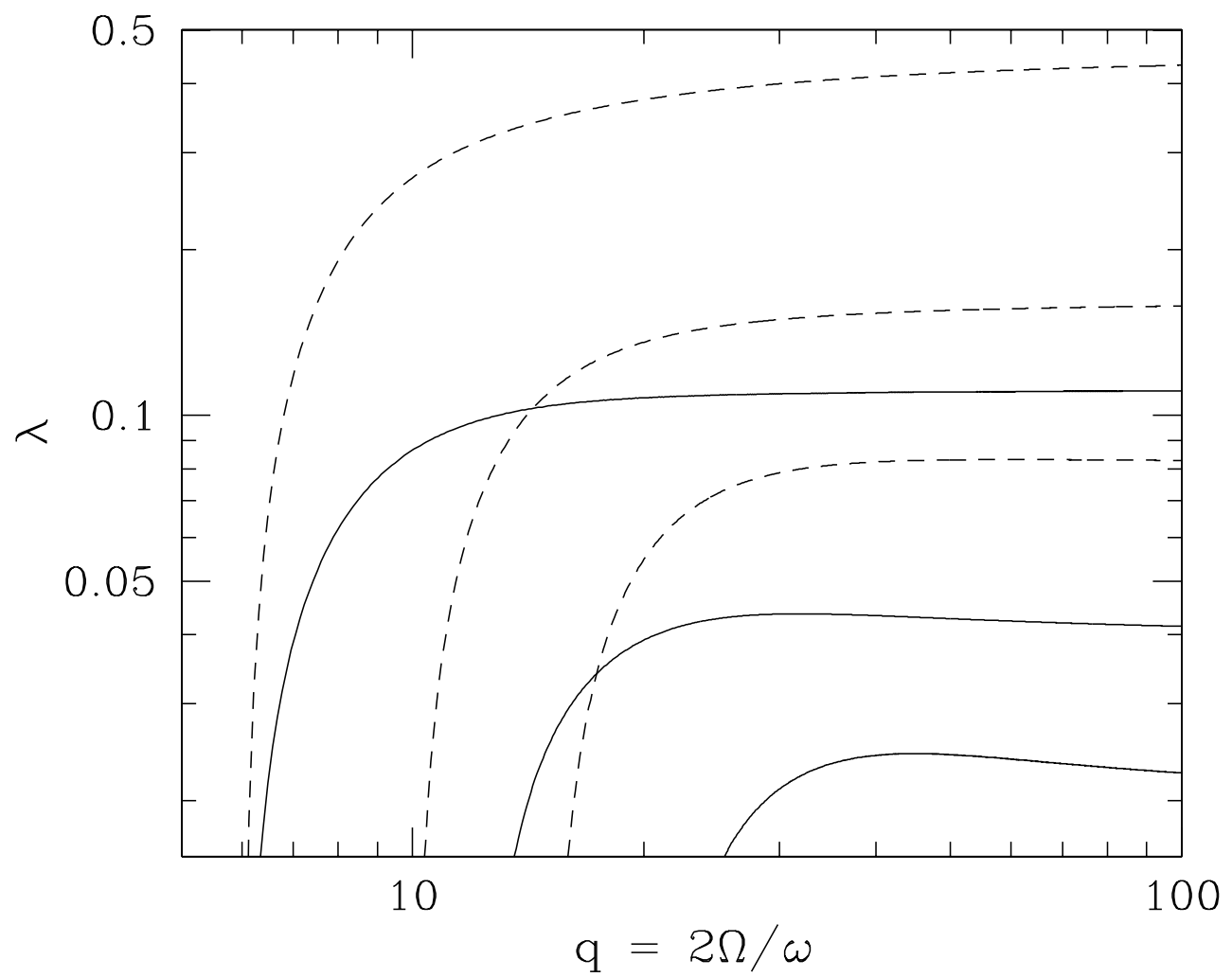


FIG. 11.— The effective wavenumber, λ , for modes on a rotating star versus the quantity $q = 2\Omega/\omega$ for three of the $m = 1$ r-modes (solid lines; from left to right, $l = 2$, $l = 3$, and $l = 4$) and three of the $m = 2$ r-modes (dashed lines; from left to right, $l = 3$, $l = 4$, and $l = 5$).

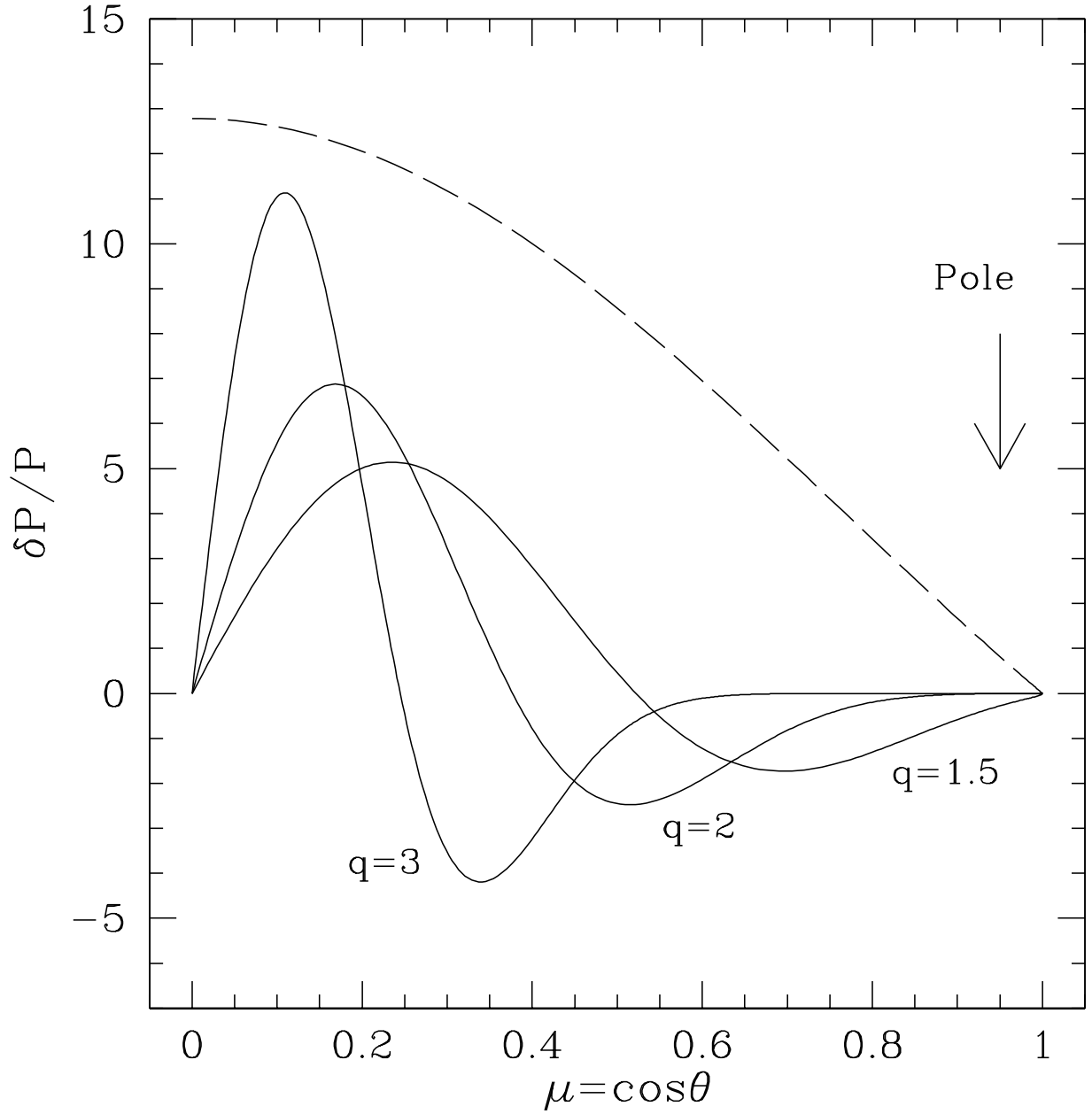


FIG. 12.— Example latitudinal eigenfunctions for four different rotationally modified modes. The solid lines denote odd parity g-modes with $q = 1.5, 2.0,$ and 3.0 . The mode amplitude is exponentially damped for $\mu \gtrsim 1/q$ and squeezed toward the equator as q increases. The dashed line shows a characteristic Kelvin mode which has a much greater latitudinal extent than the others (and always has even parity). The amplitudes of these eigenfunctions are arbitrary.

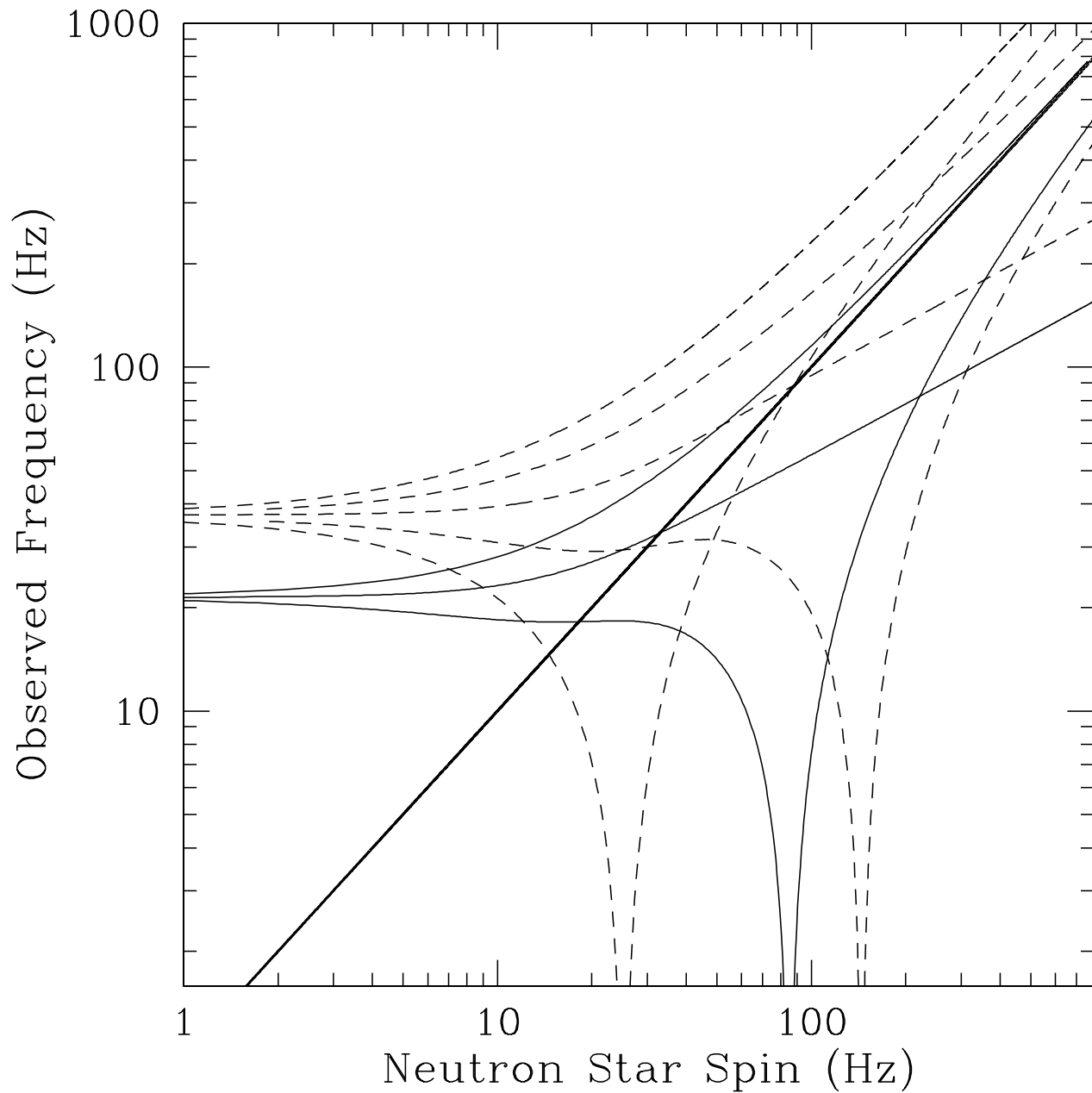


FIG. 13.— A sample of observed frequencies as a function of the neutron star spin rate for a rotationally modified $\omega_0/(2\pi) = 21.4$ Hz g-mode (frequency for a $\dot{m} = \dot{m}_{\text{Edd}}$, $F_{\text{crust}} = 1.0$ MeV/Nucleon, shallow surface wave in the non-rotating limit). Solid (dashed) lines denote modes that have $l = 1$ ($l = 2$) in the non-rotating limit. The thick solid line denotes the neutron star spin. The mode which appears closest to, and above, the spin is the $m = -1$ Kelvin mode.

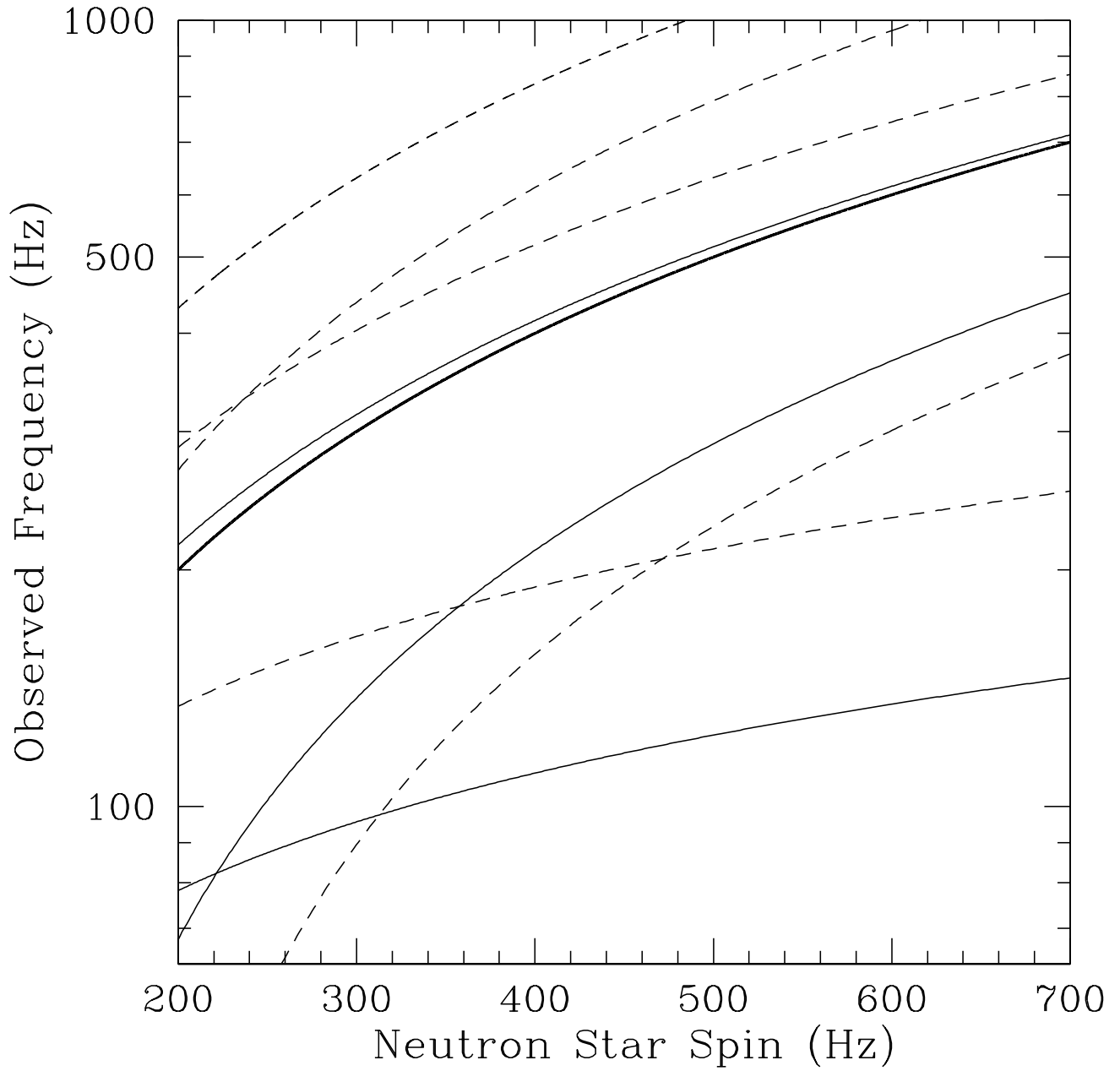


FIG. 14.— Same as Figure 13, but focusing on a range of spin frequencies that may be relevant for helium accreting neutron stars such as 4U 1820–30. If such a pattern of frequencies were seen from a neutron star it could be used to constrain properties of the star (e.g. spin and radius).